WADD-TR-60-371
Part II

A SOURCE AND DETECTOR OF RADIATION IN THE WAVELENGTH REGION 1500–50 ANGSTROMS SUITABLE FOR RADIATION EFFECTS STUDIES ON MATERIALS IN VACUO

Part II — A Study of Vacuum Ultraviolet Radiation Effects on Materials in Vacuo of Order 10^{-9}mm Hg.

TECHNICAL DOCUMENTARY REPORT NO. WADD-TR-60-371, Pt II

December 1962

Directorate Of Materials And Processes
Aeronautical Systems Division
Air Force Systems Command
Wright-Patterson Air Force Base, Ohio

Project No. 7360, Task No. 736004

(Prepared Under Contract No. AF 33(616)-6488
by Electro-Optical Systems, Inc., Pasadena, Calif.;
Horace R. Moore, H. Bernstein, and R. S. Reynolds, authors.)

NOTICES

When Government drawings, specifications, or other data are used for any purpose other than in connection with a definitely related Government procurement operation, the United States Government thereby incurs no responsibility nor any obligation whatsoever; and the fact that the Government may have formulated, furnished, or in any way supplied the said drawings, specifications, or other data, is not to be regarded by implication or otherwise as in any manner licensing the holder or any other person or corporation, or conveying any rights or permission to manufacture, use, or sell any patented invention that may in any way be related thereto.

Qualified requesters may obtain copies of this report from the Armed Services Technical Information Agency, (ASTIA), Arlington Hall Station, Arlington 12, Virginia.

This report has been released to the Office of Technical Services, U.S. Department of Commerce, Washington 25, D.C., in stock quantities for sale to the general public.

Copies of this report should not be returned to the Aeronautical Systems Division unless return is required by security considerations, contractual obligations, or notice on a specific document.

B

18-433C, 500, 1-25-63

FOREWORD

This report was prepared by Electro-Optical Systems, Inc., under USAF Contract No. AF 33(616)-6488. The contract was initiated under Project No. 7360, "The Chemistry and Physics of Materials", Task No. 736004, "The Physical Properties of Materials". It was administered under the direction of the Directorate of Materials and Processes, Aeronautical Systems Division with Mr. Robert A. Winn acting as project engineer.

This report covers work conducted from 20 December 1960 to 30 September 1961.

ABSTRACT

This report describes a space environmental research facility whereby the effects of ultrahigh vacuum and/or vacuum ultraviolet radiation on materials can be experimentally evaluated.

The facility consists of an environmental chamber of cylindrical dimensions 18" diameter x 18" depth, which is equipped with various functional and diagnostic controls, and with which is associated a vacuum ultraviolet radiation source and a radiation detector.

The radiation source is a pulsed plasma discharge which emits a line and continuum spectrum extending from the visible, through the vacuum ultraviolet, into the soft x-ray region.

The radiation detector utilizes an open photo-electron multiplier tube which is mounted in the chamber for measurements of the radiation pulse energy.

The environmental facility vacuum system includes a differentially pumped source-chamber connection and is capable of maintaining chamber pressures of order 10^{-9} mm Hg while the source is in operation.

This report includes a description of the results of some exploratory studies of the effects of ultrahigh vacuum and/or vacuum ultraviolet radiation on the characteristics of a silicon solar cell, the electrical surface resistivity of aluminum oxide, and the optical reflectance of metallic mirror coatings.

This report has been reviewed and is approved.

R. E. Brocklehurst

ROBERT E. BROCKLEHURST
Technical Director
Physics Laboratory
Directorate of Materials and Processes

TABLE OF CONTENTS

TABLE OF CONTENTS (continued)

LIST OF FIGURES

LIST OF FIGURES (cont)

I. INTRODUCTION

The program carried out at Electro-Optical Systems, Inc., under USAF Contract No. AF 33(616)-6488, has resulted in the development of an experimental facility which allows studies to be made of the effects of ultrahigh vacuum and/or vacuum ultraviolet radiation on materials. Two views of the completed space environmental research facility are shown in Fig. 1.

The present report is essentially Part II of WADD Technical Report 60-371 wherein the first phase of work on the program was reported. For simplicity, this earlier report will hereinafter be referred to as 'Part I'.

The motivation for development of the research facility has been discussed, in some detail, in Part I. Briefly, it was the need to provide a laboratory tool for simulating the in-space effects of extreme solar ultraviolet radiation on materials.

The facility can be regarded as composed of three principle elements, viz., a radiation source, a radiation detector, and an ultrahigh vacuum chamber. At the time Part I was submitted, the radiation source and detector were in the process of being assembled. They have since been completed and associated with a specially designed ultrahigh vacuum chamber to provide the research facility of Fig. 1. Subsequent sections of this report give details of the design and performance of the various elements of the environmental facility.

Three short studies have been made with the facility of the effects of ultrahigh vacuum and/or vacuum ultraviolet radiation on some typical metallic, dielectric, and semiconductor materials.

Manuscript released by the authors Sept. 1961 for publication as an ASD Technical Documentary Report.

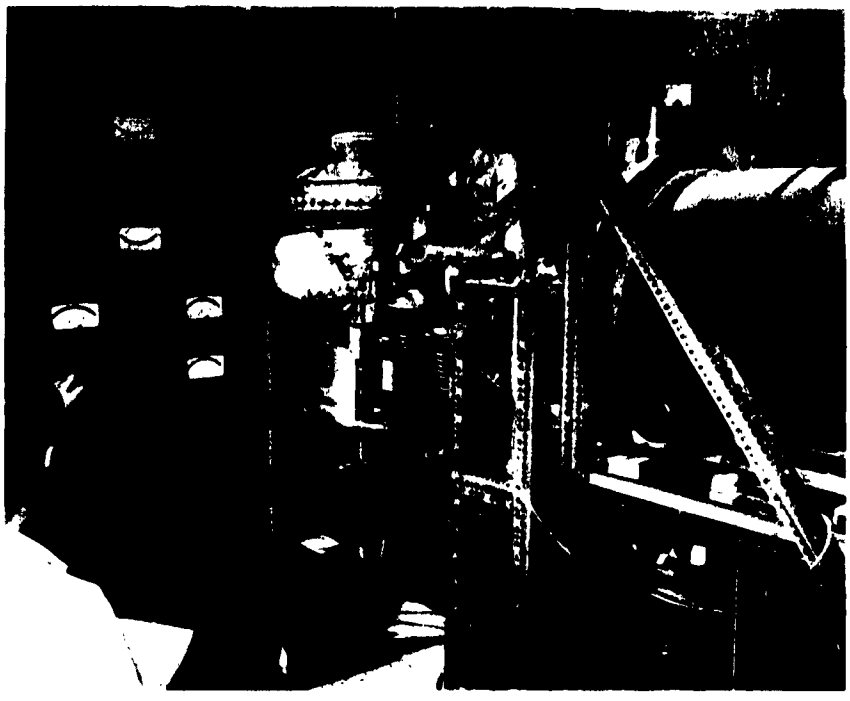

View looking towards environmental chamber with control panel in left foreground and radiation source to the right.

View looking towards radiation source with environmental chamber (enclosed in bake-out jacket) in foreground.

FIG. 1 SPACE ENVIRONMENTAL RESEARCH FACILITY

More specifically, the effects of exposure to the chamber environment of metallic mirrors, silicon solar cells, and an aluminum oxide insulator have been investigated. The results of these studies are given in later sections of this report. It must be emphasized that all of these investigations are necessarily preliminary and exploratory in their scope. The present program was not structured with the intention of proceeding in depth with the investigation of any particular environmental effect. Even so, the studies have been extremely valuable in establishing the operational capability of the research facility and have yielded results which will provide a sound basis for the further studies that are recommended in the concluding section.

Two vacuum spectrographic instruments were utilized during the development of the environmental facility. They are a Seya-Namioka monochromator and a grazing incidence spectrograph. Descriptions of these instruments are given in the appendix.

II. THE PULSED PLASMA VACUUM ULTRAVIOLET RADIATION SOURCE

The theory and basic engineering design of the radiation source were presented in Section III, Part I, together with a description of the first stages in its assembly. In the following paragraphs the final stages in the source assembly are described together with its operating characteristics. A front view of the completed source is shown in Fig. 2.

1 Source Assembly

During assembly of the source it was determined that the grossly uneven face plate surface of the energy storage capacitor was not suitable for direct mounting of the source components (See Fig. 6, Part I). Instead, a new arrangement was designed and fabricated whereby the source proper is mounted on a precisely machined polystyrene plate, independently of the capacitor, but immediately adjacent to it. The source is thus rigidly attached to an external supporting structure which enables the capacitor to be retracted without disturbing either the source alignment or the associated vacuum systems. This supporting structure can be clearly seen in Fig. 1.

On the grounded side, the cathode structure is tied directly to the capacitor external bolt circle, while the capacitor-source anode connection is made by means of three, highly conductive, flexible strips.

2 Associated Vacuum Systems

The two vacuum systems associated directly with the radiation source are the insulation vacuum system, which serves to provide electrical insulation between the anode and cathode

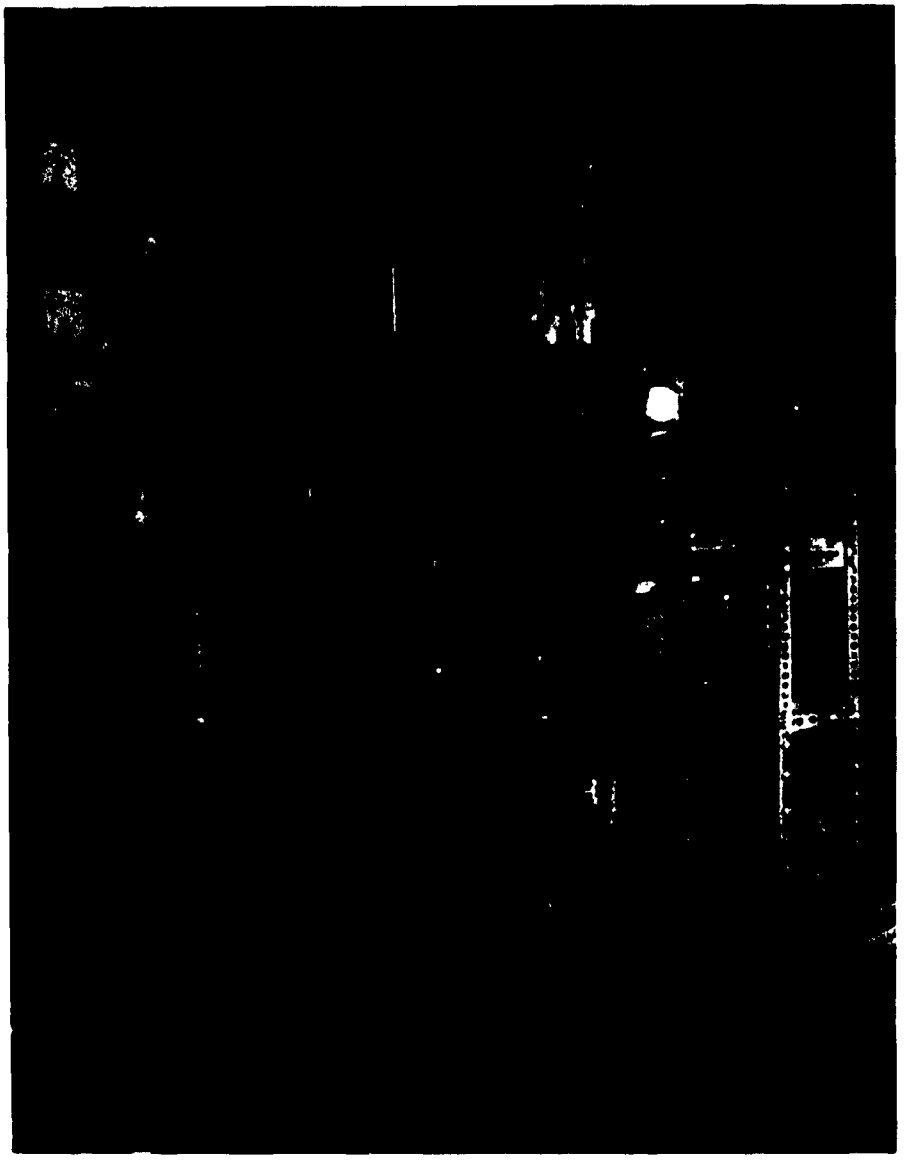

FIG. 2 VACUUM ULTRAVIOLET RADIATION SOURCE

assemblies, and the discharge vacuum system, which maintains the correct pressures in the discharge region prior to and during the source discharge.

The design requirements for the two systems have been detailed in Part I. Figure 3 shows, schematically, the structure of the completed systems. They can be seen in both Figs. 1 and 2. In the latter figure, the discharge vacuum system (3 in. Kinney diffusion pump) is in the center foreground while the insulation vacuum system (2 in. Veeco diffusion pump) is on the right.

2.1 Leak Testing

After fabrication and assembly, the systems were tested for leaks with a helium mass spectrometer type detector (Veeco MS-9). This resulted in the discovery of one critical leak, of magnitude* $>10^{-2}$ micron. liters. sec.$^{-1}$, through an extended region of a weld in the cathode assembly. This weld joins the water cooled nose of the cathode to the rest of the assembly and is in close proximity to the anode electrode (see Fig. 6, Part I). Even a small leak in this area would greatly increase the chances of breakdown in the insulation gap due to the relatively high localized gas concentration. The leak path extended from an inaccessible place in the water cooling channel to the highly polished inner surface of the cathode side of the insulation gap.

Since the chances of rewelding the porous area while still maintaining the surface requirements were not considered high, and in view of the urgency of the program schedule, a method of vacuum impregnation with a thermosetting plastic was attempted. This apparently sealed the leak, but not permanently, since it reappeared when the gap was under vacuum for several days. After several similarly unsuccessful attempts to seal the leak with the plastic material, glyptal was resorted to. This material did plug the leak, reducing its value to below 10^{-7} micron. liters. sec.$^{-1}$ which is the limit of sensitivity of the detector.

---

*Since a mechanical pump had to be operated in parallel with the leak detector when working with this leak, its actual magnitude could not be determined.

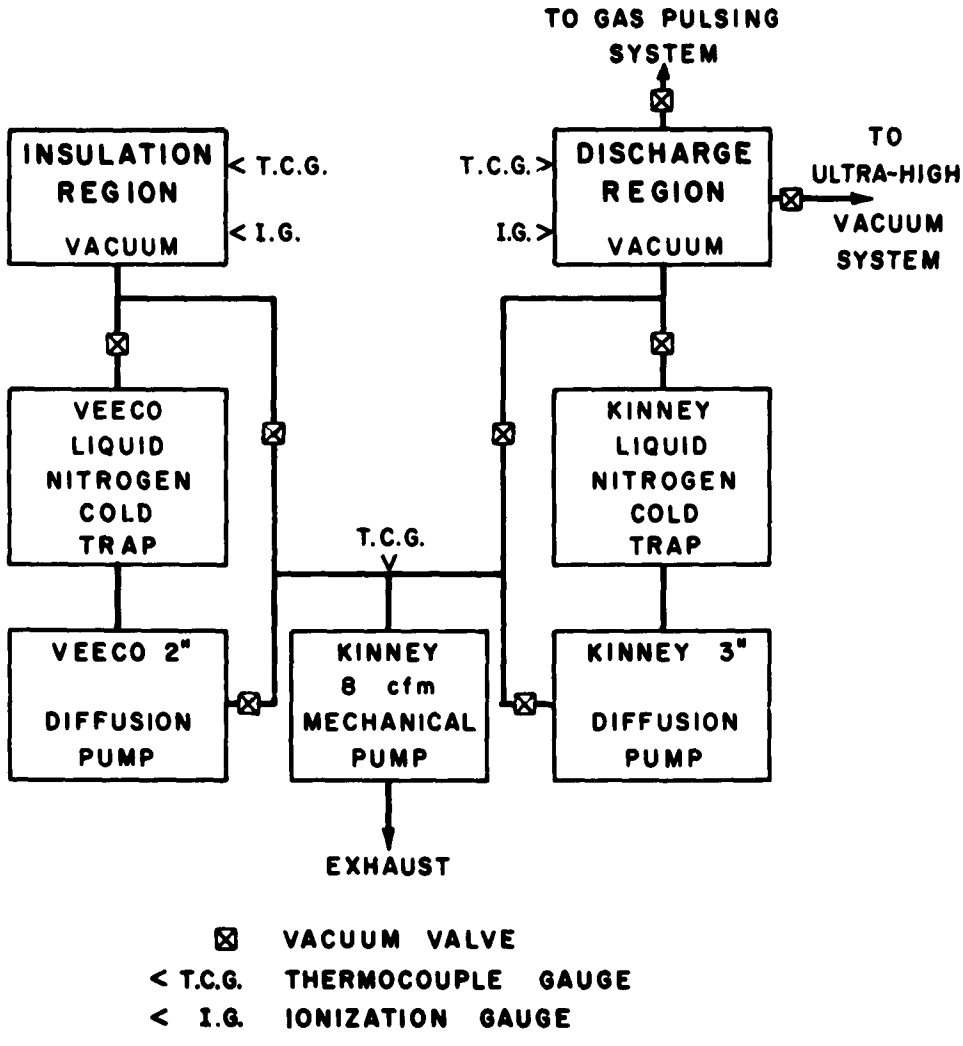

FIG. 3 SCHEMATIC DIAGRAM OF RADIATION SOURCE VACUUM SYSTEMS

2.2 Vacuum System Performance

Initially, the ultimate pressures of the two diffusion pumps were checked when valved off on their high vacuum sides. Both systems reached between 10^{-6} and 10^{-7} mm Hg.

The insulation region system was designed to reduce the pressure to about 10^{-6} mm Hg in the coaxial gap. The ultimate pressure actually reached on testing, for reasonable pumping times, was 8×10^{-6} mm Hg. This was ascribed to the large surface area to volume ratio in the insulation gap, and the fact that these surfaces could not be baked out to accelerate release of surface contaminants. As will be shown in part 5 of this section, it was found that an insulation pressure of only 10^{-5} mm Hg was sufficient to withstand the design operating voltage of 50 kv. The failure to reach the design pressure of 10^{-6} mm Hg was accordingly not serious.

The discharge region system performed very well on test, a pressure of 10^{-6} mm Hg being reached in the discharge tube. The performance of this system during actual source operation is described in part 4 of this section.

3 Associated Electrical Equipment

Upon completion of all electrical connections concerning the source proper, the capabilities of the power supply and energy storage capacitor were determined.

The capacitor was charged with the Sorenson power supply and found to operate successfully to 55 kv, 5 kv above the design operating voltage. The charging rate of the capacitor was determined approximately for different values of applied voltage.

The discussion in Part I suggested maximum pulse rates approaching one per sec. This was calculated with the assumption that the delivery voltage remained constant, i.e., that the power supply

regulation was perfect. In fact, no power supply has perfect regulation and, in view of the voltages and currents required in this application, poor regulation was anticipated. However, it was not expected that the regulation would be as bad as the experiments subsequently showed. With a delivery voltage of 50 kv the power supply could charge the capacitor to 50 kv in about 40 sec. With a delivery voltage of 55 kv the time to charge to 50 kv was reduced to about 25 sec. There is a possibility that the charging time can be further decreased by adjusting some of the power supply circuit parameters but the order of pulse rate will still be near two per minute if the capacitor is charged to full voltage. As results presented in later sections indicate, the source does operate successfully at less than maximum available voltage and this fact provides a means of increasing the pulse rate if necessary.

4 Gas Pulsing System

The principle of the gas pulsing method has been discussed in Part I. Briefly, it is required to introduce enough gas into the evacuated discharge region of the radiation source to cause cascading ionization, and then to evacuate the region to an insulating condition before the voltage can again build up.

The different components comprising the gas pulsing system are depicted in Fig. 4. Through suitable control devices a regulated helium tank supplies pressurized helium to a charging volume (approximately 2 liters) containing a liquid nitrogen cooled, activated charcoal trap for removal of any inpurities from the gas. Before charging, the system is evacuated with a mechanical pump.

The purified helium is fed to a three-way solenoid valve with one outlet blanked off. The blanked-off section serves as a measuring volume (approximately 2 cc) for the actual gas pulse. When the valve is closed the measuring volume is open to the charging volume. When the valve is opened, the charging volume is cut off from the valve and the measuring volume is opened to the discharge region, thus providing the desired gas pulse. The quantity of gas in the measuring volume is

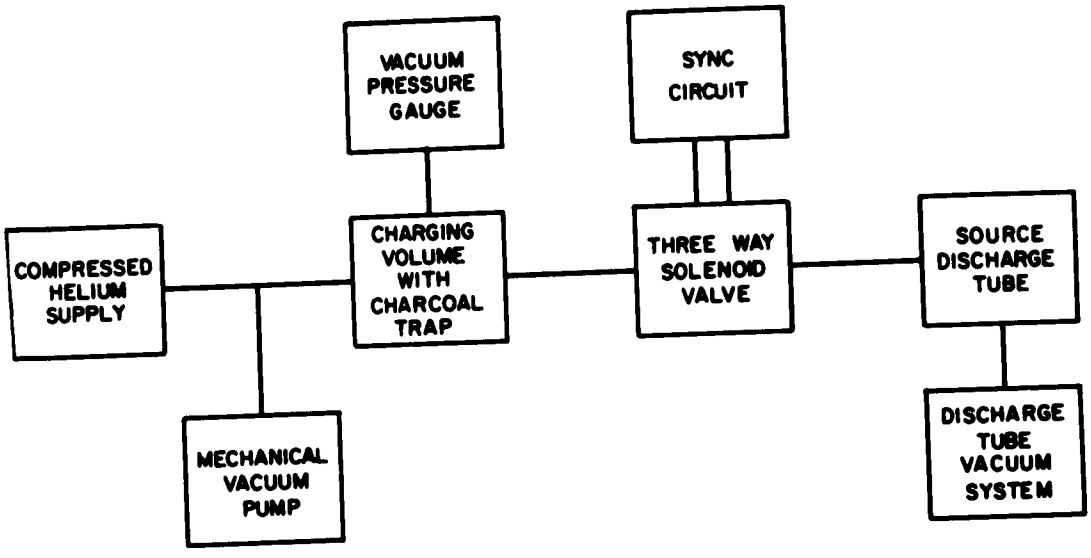

FIG. 4 GAS PULSING SYSTEM

controlled by the pressure in the charging volume. The proper charging pressure to actuate the discharge is determined experimentally.

The experimental results obtained with this method of pulsing have been quite satisfactory. Initially, static pressure tests using first air and then helium were performed in order to determine the actual discharge pressures as a function of voltage. As expected, the discharge occurred at lower pressures for air than for helium. In both cases, the discharge pressure was effectively constant for voltages between 10 kv and 50 kv. As the voltage was reduced below 10 kv, the discharge pressure rose gradually.

In Part I, the predicted value for breakdown using helium was given as being slightly above 5×10^{-2} mm Hg. The actual values have varied slightly around 10^{-1} mm Hg for voltages above 10 kv. For air, the breakdown pressures were about $1 - 2 \times 10^{-2}$ mm Hg.

After completion of the static tests, the automatic solenoid valve was introduced and the effect of the gas pulse on the performance of the discharge vacuum system was determined. Because the gas pulsing cycle occurs at such a rapid rate, the vacuum gauges cannot follow the pressure changes accurately. Their readings probably lag the actual pressure by a considerable amount. For this reason, an exact analysis of the pulsing - pumping capabilities is not possible. In a typical test, the discharge pressure before pulsing was approximately 10^{-5} mm Hg. The gas pulse moved the pressure reading to about 10^{-2} mm Hg in about 1/2 sec, the discharge occurring immediately upon gas injection. The pressure reading then fell to about 10^{-4} mm Hg, well below the vacuum needed for insulation, in about 1-1/2 sec. after gas injection. The actual pressure changes were, of course, much more rapid.

The fast pump-out times achieved in such tests indicated that the gas load from the radiation source into the ultra-high vacuum system would be compatible with the design requirements of Part I.

5 Operational Performance of Radiation Source

The first stage in evaluating the operational performance of

the source was to determine its voltage handling capability. The radiation source, initially, was electrically detached from the capacitor so that if any mishap occurred, a large quantity of stored energy would not create further problems. The insulation and discharge vacuum regions were both pulled down to a pressure of approximately 10^{-5} mm Hg and the voltage slowly applied to the anode of the source. When the voltage reached a value of 15 kv sparking started to occur in the insulation vacuum region, a pressure pulse occurring simultaneously with each spark. After the sparking had subsided and the pressure stabilized, the voltage was increased in steps of 500 - 1000 volts. Each step was accompanied by sparking and pressure rises. After more than 24 hours of such conditioning of the electrodes a voltage greater than 50 kv was reached. The voltage was then oscillated between zero and 50 kv with no evidence of sparking or pressure pulses. The static pressure tests on the breakdown point, described in the previous section, were carried out at this time.

At the conclusion of the static pressure tests, the source was connected electrically to the capacitor. Several shots were then fired with an applied voltage of 25 kv, Fig. 2 being an actual photograph of the source when discharging. Light can be seen emerging from the blank-off window which is located approximately 5 inches from the ceramic discharge tube. The photograph is a double exposure. Since the camera could not easily be synchronized with the discharge, the first exposure was taken with an open shutter in a darkened room. Only the light from the source was visible. After the first exposure, the lights were turned on and a second exposure was taken of the radiation source.

The source was next dismantled to allow examination of any deleterious effects of the discharges. Small quantities of material were found to have been transferred from the anode to the cathode in the area of the discharge. Even greater evidence of material transfer was seen on the blank-off window after a planned discharge. Only 3 or

4 discharges were necessary to render the blank-off window opaque from a deposit of the aluminum electrode material when the source was fired at about 25 kv. The anode electrode, from which most of the material was coming was deeply eroded and fused to the ceramic discharge tube. From the nature of the deposit on the blank-off window, it was concluded that the aluminum was molten when it hit the window. The window itself was chipped and marred, possibly due to the extremely fast cooling of the molten aluminum.

As a step towards obviating the erosion of electrode material, with its subsequent ejection from the source, a new anode electrode was fabricated from molybdenum. During this time, the source apparatus was relocated opposite the slit of the grazing incidence vacuum spectrograph.

After the source had been assembled with the new molybdenum electrode, tests were run to determine the critical voltage at which material would be ejected from the source. With the molybdenum anode and an aluminum cathode, material started to appear on the window with discharges at voltages of about 12 kv. At higher voltages, it was discovered that most of the deposited material was from the aluminum cathode. The molybdenum anode had cut down the anode sputtering by a discernible amount but, at high voltages, the sputtering was still too great for the radiation source to be used directly with the spectrograph without endangering the slit and grating. Since the tests showed that if the source were operated at voltages less than 12 kv no material would be emitted during discharge, the source was connected to the spectrograph with the intention of obtaining a spectrogram for 10 kv operation. During this series of tests, it was observed that the high voltage condition of the insulation gap surfaces was quickly lost on exposure to air at atmospheric pressure. This necessitates carefully re-conditioning the surfaces by slowly increasing the applied voltage as previously described. It is considered that hard anodizing all of the aluminum surfaces exposed to the insulation vacuum would probably reduce the chances of electrical breakdowns occurring in the gap.

6 Source Emission Characteristic

The blank-off window mentioned in the previous section was removed from the source discharge chamber and a vacuum bellows connection placed between the source and the entrance slit of the vacuum spectrograph. With this arrangement, the spectrograph and discharge tube shared a common vacuum, separated by the impedance of the slit. The source tube was aligned on an optical axis through the grating center and slit, and at a distance of approximately 40 cm from the slit.

With the spectrograph evacuated to about 10^{-5} mm Hg, three exposures were recorded on Kodak SWR coated 35 mm film, the slit width in all cases being 20 microns. The resultant spectrograms of the source emission, details of which follow, were very successful.

While further confirming experiments must yet be performed, the presently available data evidence a strong emission of continuum and line radiation from wavelengths at least as short as λ50 and extending through λ1500 to longer wavelengths. These results were obtained with only 1/25 of the total available energy/discharge.

All three exposures were taken with a capacitor or discharge voltage of 10 KV to minimize possible damage to the slit and grating by ejected material. The first exposure was for a single discharge and even this was sufficient to give lines and a discernible continuum in the approximate region λλ50 - 500.

The spectrogram resulting from the second exposure, which was for 20 flashes, is reproduced in part as Fig. 5. Here a strong continuum with superimposed line radiation is evident in the approximate region λλ50 - 1500.

The third and final spectrogram recorded during these tests was identical with the previous 20 flash exposure except that a BSC-2 glass filter was placed over the spectrograph slit. Such a filter prevents all radiation shorter than about λ3000 from reaching the grating. This experiment was designed to eliminate the possibility that the observed continuum was not genuine but was due to stray and scattered

light of longer wavelengths. The resultant spectrogram was completely blank which confirms the reality of the continuum, at least to the extent that no scattered radiation of wavelengths $>\lambda 3000$ was present.

No opportunity could be taken, at this time, to pursue the more detailed spectroscopic studies which would be necessary to more certainly establish the nature of the source emission. It is quite possible that short wavelength scattered radiation contributes to the continuum observed with the grazing incidence spectrograph. The effects of order overlap, film response, and grating efficiency on the recorded data should also be evaluated in a more definitive study.

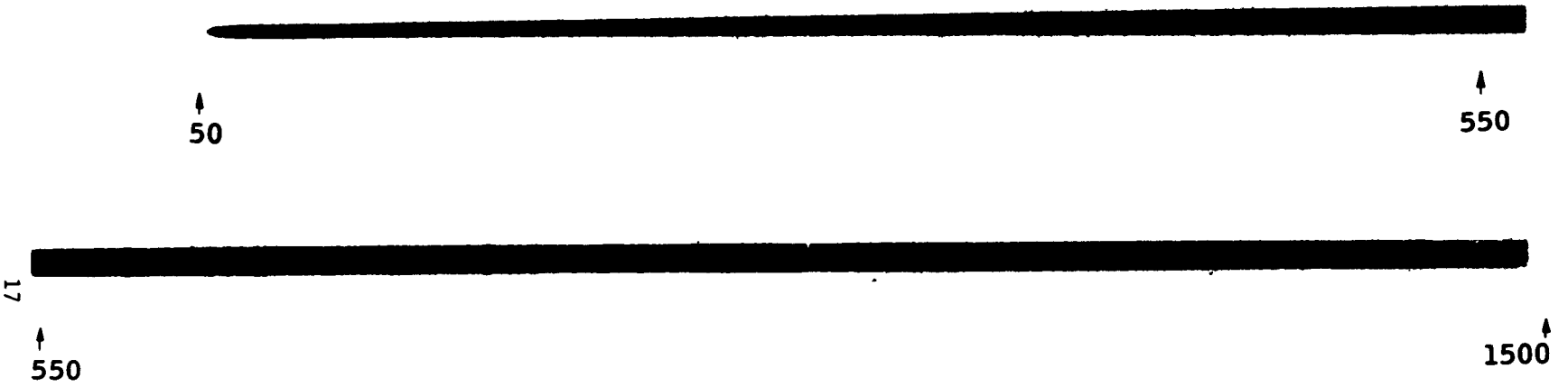

FIG. 5 SPECTROGRAM OF EMISSION FROM THE RADIATION SOURCE RECORDED WITH THE GRAZING INCIDENCE VACUUM SPECTROGRAPH

III. THE OPEN PHOTO-ELECTRON MULTIPLIER DETECTOR SYSTEM

The reasons for choosing an open (windowless) photo-electron multiplier tube as the sensor in the detector system developed for use with the radiation source have been given in Part I. The actual tube used is the 14-stage DuMont SP-206 which is supplied on special order by the DuMont Laboratory Inc. This tube has a pure nickel cathode and beryllium-copper dynodes. In developing the detector system circuitry to be associated with the photomultiplier tube various tests and experiments have been performed. These fall into two classes: viz., those performed prior to the assembly of the ultra-high vacuum chamber system, and those performed subsequently as an integral part of the source-chamber complex. They are referred to in the following sections as "pre-chamber" and "in-chamber" experiments respectively. In the latter case, the main detector function is the measurement of the radiant energy in a given source pulse. This is accomplished with an integrating type detector circuit.

1 Pre-Chamber Detector Evaluation

The photomultiplier dynode structures are received from the manufacturer in a glass vacuum envelope. In the pre-chamber experiments, a structure was completely removed from its glass envelope and mounted inside a small cylindrical vacuum chamber. This chamber was fabricated from aluminum (black anodized) and designed to be attached to the exit slit port of the Seya-Namioka vacuum monochromator. It is shown thus mounted in Fig. 28. The vacuum valve seen between the photomultiplier chamber and the monochromator port serves to isolate the dynode structure from the monochromator chamber. The opposite end of the dynode chamber is essentially an 18-wire feedthrough header by means of which the electrical connections are made to the dynodes. The associated voltage dividing network components are mounted outside

the dynode vacuum and immediately adjacent to the header. They are covered with a shielding canister from which the main connecting leads are seen to protrude in Fig. 28.

1.1 Pre-Chamber Detector Circuit

There are two possible modes of applying the high tension necessary for the electron multiplications, viz., a negative or positive supply. A disadvantage of the latter lies in the necessity of using a coupling capacitor of high working voltage. Direct coupling from the plate of the photomultiplier to subsequent equipment would result in chassis potentials far above ground. These difficulties are avoided by the use of a negative supply.

A schematic of the circuit used in the pre-chamber work is shown in Fig. 6. The cathode is kept at the negative supply voltage while the anode end is grounded. Normally, the anode is at ground potential; however, an electron flow through the plate load resistor will cause the plate to go negative. For pulsed operation, a negative pulse will appear at the output.

The accelerating voltages were obtained from a Hamner Model N-413 Power Supply by means of a voltage dividing network, as shown in Fig. 6. The choice of resistance values was based on the following considerations:

1. The total current through the network should be at least 10 times the maximum average current collected at any one dynode.
2. The voltage between cathode and first dynode should be kept considerably higher than the succeeding stages for optimum signal-to-noise ratio.

1.2 Detector Noise Characteristics

The noise characteristics of the photomultiplier were investigated as a function of the supply voltage. The output was simultaneously fed to a Tektronix oscilloscope (Model 545) and a

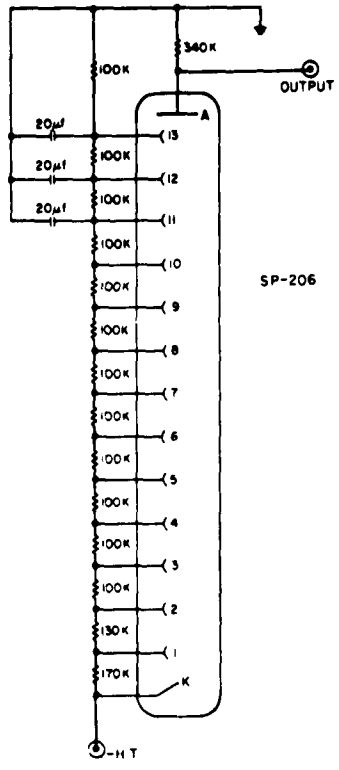

FIG. 6
THE PRE-CHAMBER
DETECTOR CIRCUIT

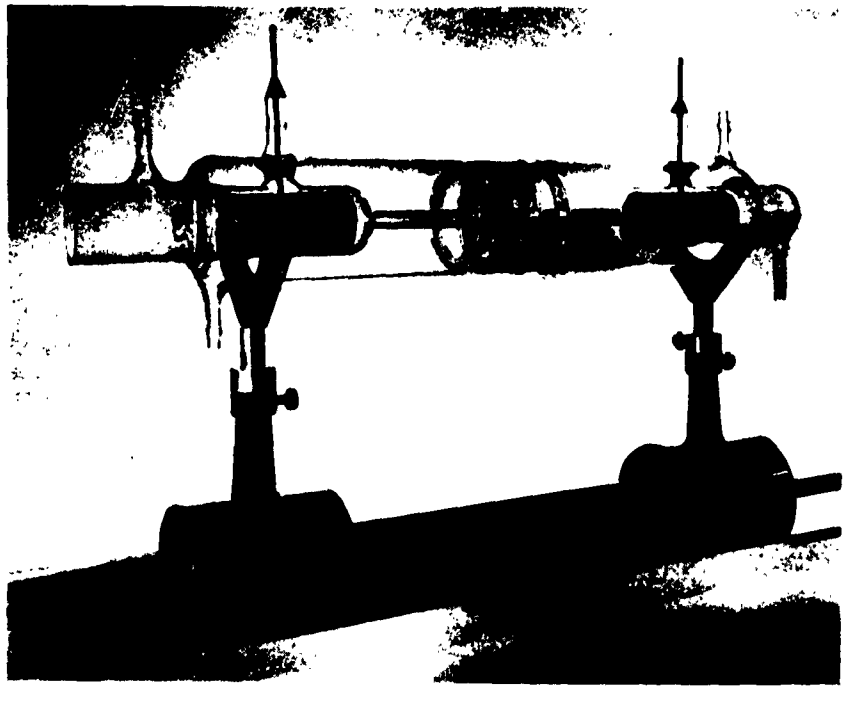

FIG. 7
CAPILLARY GAS DISCHARGE
RADIATION SOURCE

Keithley Electrometer (Model 610A). The maximum sensitivity of the oscilloscope was 5 mv/cm while that of the electrometer was 0.1 mv/division.

With the photomultiplier dynode structure exposed to the atmosphere, no output could be detected on either instrument at supply voltages up to 4000 v. It was conjectured that collisions between photoelectrons and air molecules prevented any collection at the anode.

The detector was then attached to the exit slit port of the vacuum monochromator. At a pressure of approximately 10^{-2} mm Hg., it was observed that high voltage breakdown occurred at about 500 volts. As expected, a vacuum of better than 10^{-4} mm Hg. was essential before the supply voltage could be raised sufficiently high to allow a detectable output. Under the conditions of a vacuum of 8×10^{-5} mm Hg. and a supply voltage of 2400 volts, the average noise level was 2 mv, which corresponded to an anode current of 6×10^{-9} amps. Such small dark currents were anticipated because of the high work function of Ni (5 eV).

1.3 Pressure Limitations on Detector Operation

It was established in the preceding section that the maximum voltage that can be applied to the photomultiplier without breakdown is critically dependent on the degree of vacuum within the detector chamber. This fact is reflected of course, in the maximum gain permissible under given operating conditions.

At the time the noise studies were undertaken, the cathode was saturated by gas adsorption. As a result, the photomultiplier voltage could not be raised to values considered necessary for sufficient output. The tests indicated that a vacuum of better than 10^{-5} mm Hg is necessary for operating the photomultiplier at voltages above 3000 volts.

1.4 Spectral Response of Detector

The spectral response of the photomultiplier detector to a radiation source was investigated. For this purpose, the capillary gas discharge source shown in Fig. 7 was designed and fabricated.

This source has cylindrical aluminum electrodes, through one of which the capillary source is viewed. A cooling water jacket with integral expansion bellows surrounds the capillary. Using helium gas the source operates, typically, at 1000 volts A.C., the current being about 0.25 amperes.

The discharge tube was directly attached to the entrance slit port of the vacuum monochromator as shown in Fig. 28. Both the entrance and exit slits were opened to their full width of 500 microns. It was found that with this arrangement, the best vacuum obtained in the chamber (without too much sacrifice in intensity) was about 5×10^{-4} mm Hg. The corresponding breakdown voltage was approximately 1400 volts.

To reduce the gas load entering the monochromator from the discharge tube, a lithium fluoride lens was inserted between the source and entrance slit. The monochromator could then be evacuated to about 7×10^{-5} mm Hg. Correspondingly, the supply voltage remained stable at 2800 volts, at which point the average detector output was well above the noise level. A block diagram of the detection apparatus is shown in Fig. 8. The output of the Keithley Electrometer was fed to a Speedomax pen recorder (Model G).

During the course of the experiments being described, the monochromator vacuum gradually improved. This was attributed to outgassing in the photomultiplier structure. Spectra were recorded when the pressure leveled off at about 3.5×10^{-5} mm Hg. A strip chart record of a typical scan is shown in Fig. 9.
Because of absorption in the lithium fluoride lens, the response below λ1100 was virtually nil. As a result, only first order lines appeared between λ1135 and λ1744. Of these, the strong lines were identified as: H(λ1216), O(λ1305), N(λ1201, λ1494, and λ1743), and C(λ1562 and λ1657).

With improved conditions another attempt was made at recording the source spectrum without the lithium fluoride lens. The

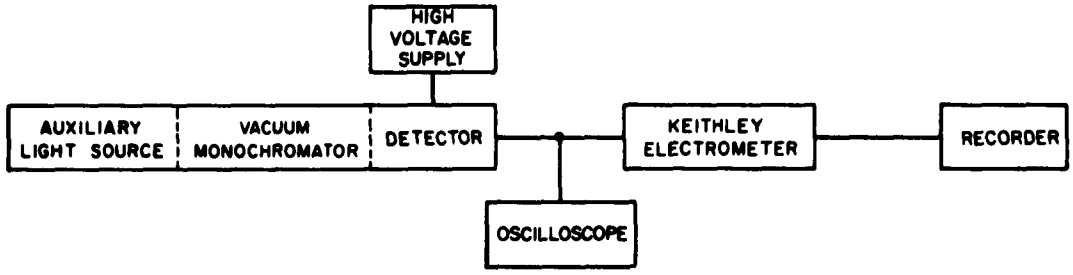

FIG. 8 BLOCK DIAGRAM OF PRE-CHAMBER DETECTOR SYSTEM

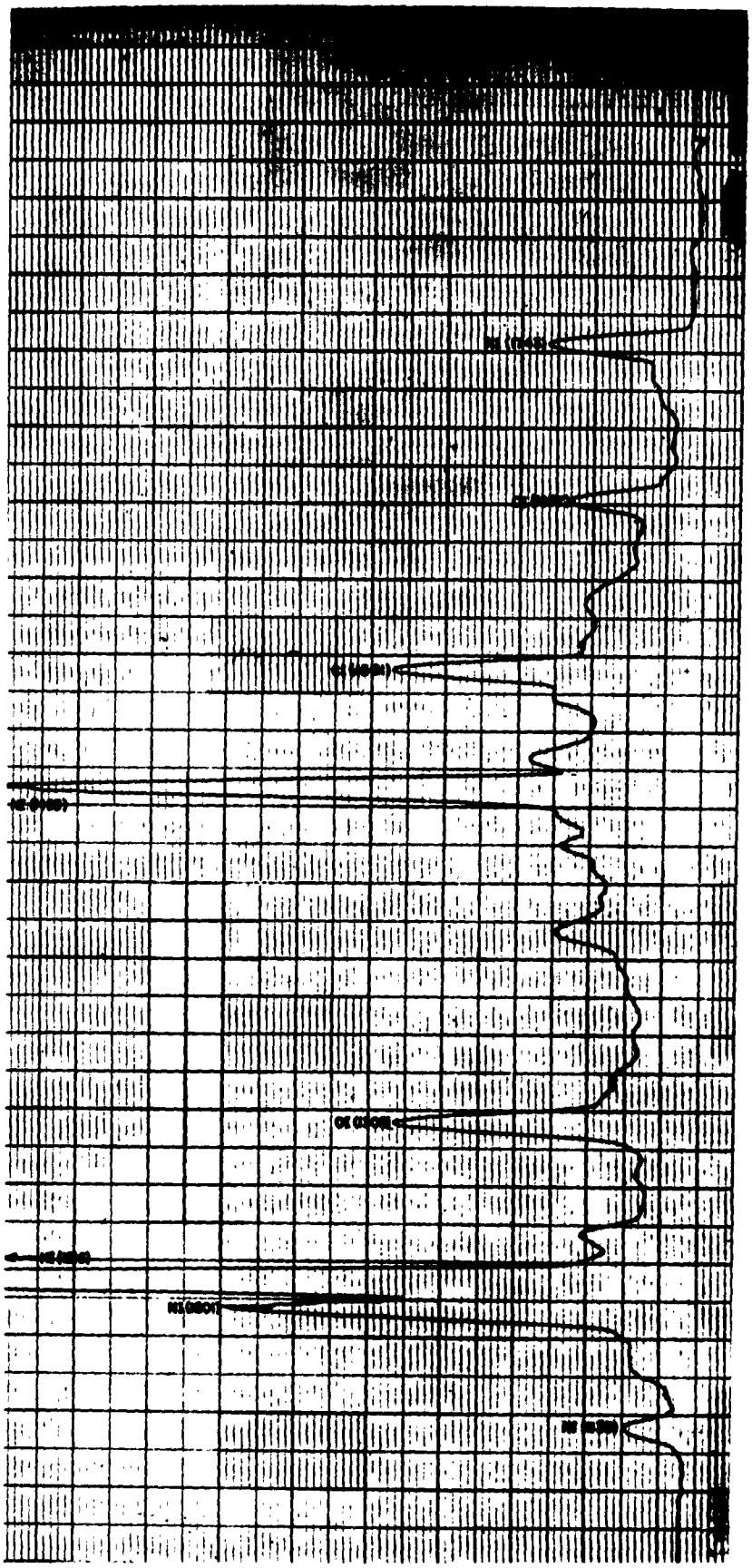

FIG. 9 OPEN PHOTOMULTIPLIER DETECTOR SPECTRAL RESPONSE CURVE FOR A HELIUM DISCHARGE (LiF Lens)

source slit width was reduced to 200 microns as an additional aid in securing a working vacuum. At the expense of intensity, proper operation was achieved with a chamber pressure of 3×10^{-4} mm Hg and a supply voltage of 2700 volts. The results are shown in Fig. 10.
The spectral response of the detector has now been extended down to approximately 580 Å which lies near the lower limit of the monochromator. The identified lines are: He(λ584 and the second order at λ1168), H(λ936, λ950, λ972, λ1072, and λ1216),N(λ1088, λ1100, λ1135 and λ1201), and O(λ989, λ1027, λ1040, and λ1305).

The above results have been compared with spectrograms such as that of Fig. 29 and found to be in excellent agreement.

1.5 Photomultiplier Amplification

The gain of the photomultiplier was determined directly by measuring simultaneously the cathode photo-emission and the anode current. The former was measured by inserting the Keithley Electrometer (used as a micro-microammeter) in series with the cathode.

With 2800 volts applied across the photomultiplier and the Lyman-α line of hydrogen at λ1216 incident, the peak anode current was 1.3×10^{-7} amps., and the cathode current 1.4×10^{-12} amps. This yields an amplification of 9×10^{4}.

1.6 Detector Sensitivity

The weakest signal that the photomultiplier can certainly detect is equivalent to an anode voltage of approximately 4 mv (see Section 1.2). Taking an amplifier gain of 10^{5}, the corresponding cathode emission current will be about 10^{-13} amperes. The quantum yield of Ni, after suitable cathode conditioning (see Ref. 1) is 0.02 photoelectrons/photon in the range $\lambda\lambda$1200-400. This indicates that the minimum detectable photon flux will be approximately 3×10^{7} photons/sec.

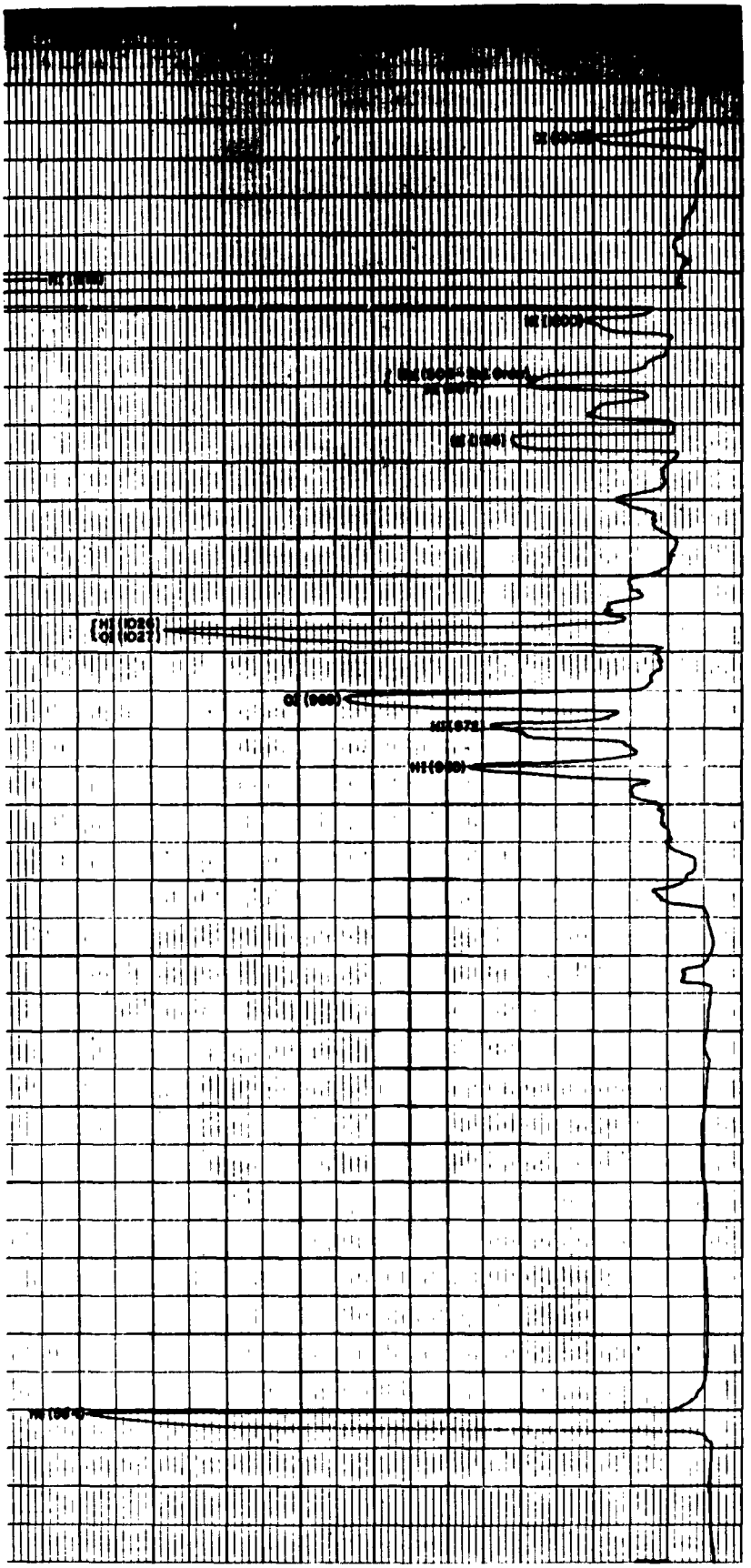

FIG. 10 OPEN PHOTOMULTIPLIER DETECTOR SPECTRAL RESPONSE CURVE FOR A HELIUM DISCHARGE

2 In-Chamber Detector Development

The feasibility and various characteristics of the SP-206 open photomultiplier as a detector of V.U.V. radiation were established in the preceding sections, prior to installation of the ultra-high vacuum environmental chamber. A new photomultiplier header and related structure was assembled for use in the chamber. This is shown in Fig. 11. It is seen that the glass envelope was kept intact, except for the window, which was cut off just prior to pump-down of the environmental chamber. This facilitated the mounting of the photomultiplier on the header which will be described in Section IV.

The design provides means for attaching collimators in front of the cathode, alignment of cathode and collimator with respect to the incident beam, and for the insertion of various test samples between the collimator and the cathode. This arrangement guarantees that the same quantity of radiation is incident upon test samples as upon the photocathode during irradiation studies in the chamber. Electrical connections between the flexible photomultiplier electrode leads and the header feed-through wires were made with the detachable couplers visible in Fig. 11.

2.1 In-Chamber Detector Circuit

The previously developed detector circuit (see Fig. 6) was modified as shown in Fig. 12, when the photomultiplier was mounted for use in the environmental chamber. A mechanical requirement of the external circuitry is that it can be removed from its operating position on the outside of the photomultiplier header during bake-out of the main chamber. This is accomplished by mounting all components in a shielding box provided with an array of banana jacks which plug into their counterparts attached to the header feed-throughs.

As shown in Fig. 12, the detector circuit includes an integrator on the output side. Its purpose is, of course, to

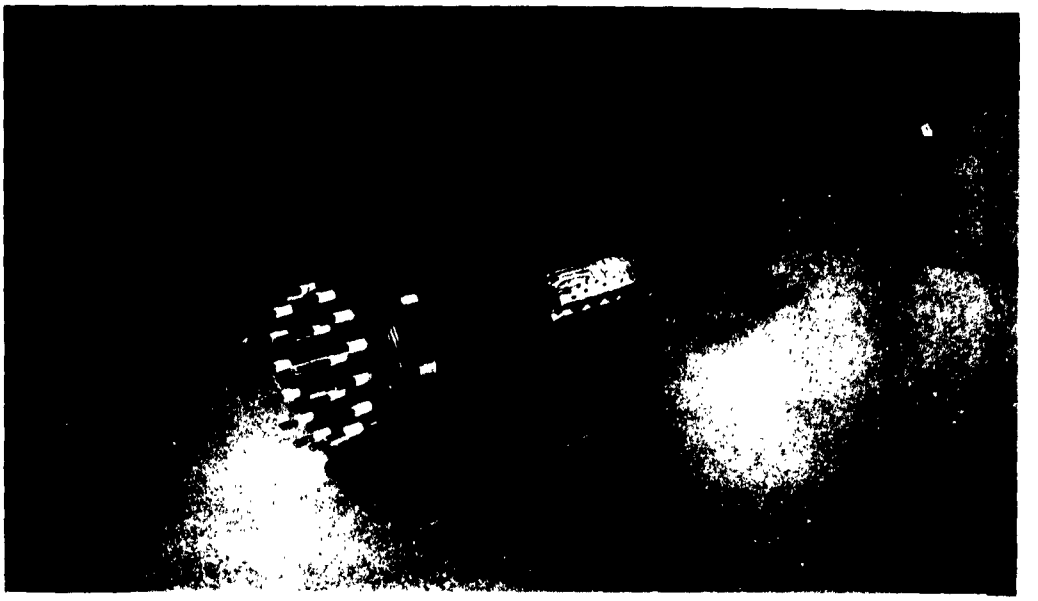

FIG. 11 IN-CHAMBER ASSEMBLY OF OPEN PHOTOMULTIPLIER DETECTOR

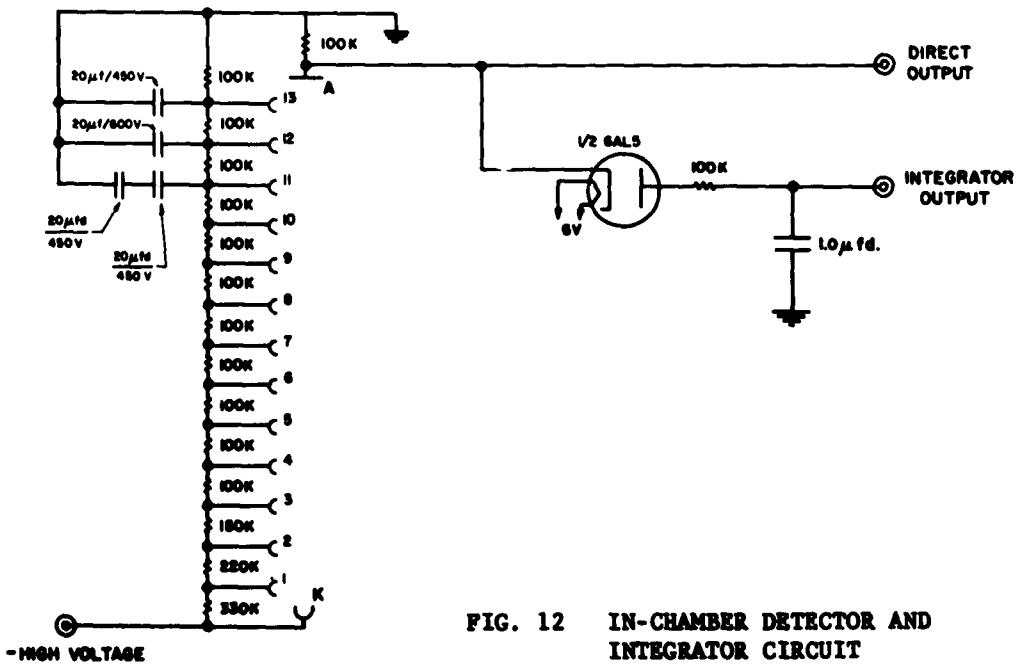

FIG. 12 IN-CHAMBER DETECTOR AND INTEGRATOR CIRCUIT

allow determination of the radiant energy per pulse from the V.U.V. radiation source. The principle of operation of the integrator is now discussed.

When a radiation pulse is incident upon the cathode of the SP-206 photomultiplier, a corresponding voltage pulse, v(t), appears at the anode. At any time, t, during the passage of the pulse, the differential equation governing the flow of charge, q, to the integrator capacitor is

$$R \frac{dq}{dt} + q/C = v(t). \qquad (1)$$

R is the resistance of the vacuum tube diode in the forward direction plus any added series resistance, and C is the capacitance of the integrator capacitor.

A solution to equation (1) is

$$q(t) = \frac{1}{R} e^{-t/RC} \int_0^t v(t)\, e^{t/RC}\, dt. \qquad (2)$$

If the product RC is made large with respect to the duration of the pulse, $e^{t/RC} \approx 1$ over the whole integration, and the solution simplifies to

$$V_C = q/C = \frac{1}{RC} \int_0^\tau v(t)\, dt, \qquad (3)$$

where V_C is the resultant voltage across the integrator capacitor after the passage of the pulse and τ is the pulse duration.

As will be shown by the measurements presented in Section V, the duration of the radiation source pulse is of the order of 10^{-3} sec. With an integrator capacitance of value C = 1μFd, and a diode forward resistance of about 2500 ohms, the requirement that $RC \gg \tau$ was met by placing a 10^5 ohm resistor in series with the diode. This increased the effective forward charging time constant RC, to 0.1 sec., or about one hundred times the pulse duration, τ.

During operation of the integrator circuit, an increment is noted on its read-out device for each pulse of the radiation source. The diode, which has a resistance greater than 10^9 ohms in the reverse direction, assures negligible leak-off (between pulses) through it, while the Keithley Electrometer offers 10^{14} ohms input impedance for a similar behavior.

Now, the voltage appearing across the plate load resistor, v(t), is directly proportional to the intensity of the radiation falling upon the cathode. Equation (3), which is concerned with the area under the voltage vs. time curve, and thus the integrated intensity, provides a measure of the energy in a pulse of radiation.

2.2 High Voltage Testing of Detector

The first stage of high voltage testing involved the external circuitry alone. It was found that no breakdown occurred for applied voltages up to 4500 volts.

With the photomultiplier header feedthroughs plugged into the box, and thus electrical connection made to the photomultiplier leads, the high voltage tests were continued. At this stage, the window of the glass envelope surrounding the photomultiplier had not been removed and the pressure within was not known. There was internal arcing (within the dynode structure) at 2670 volts.

Finally, the complete detector assembly was attached to the environmental chamber, the window of the glass envelope removed, and the system pumped down to an ultra-high vacuum of order 10^{-9} mm Hg. At this low pressure, no breakdown occurred for voltages as high as 4500 volts. The tests did not go beyond this value, as this is more than adequate for satisfactory operation of the photomultiplier.

IV. THE ULTRAHIGH VACUUM ENVIRONMENTAL CHAMBER SYSTEM

When the development of the radiation source and detector had proceeded to the point that their feasibility was established, a subcontract was issued to the Radio Corporation of America Industrial Tube Products, Lancaster, Pennsylvania, for the ultra-high vacuum environmental chamber system. As discussed in Section I, the purpose of this system is to provide a chamber wherein materials can be irradiated with vacuum ultraviolet radiation at pressures of order 10^{-9} mm Hg. The system was delivered by the Radio Corporation of America and installed at Electro-Optical Systems in October, 1961.

The schematic diagram of Fig. 13 shows the relative arrangement of the radiation source and the two major sections of the chamber system. These latter are the differential pumping system and the research chamber proper. The research chamber itself is capable of operating at ultra-high vacuum, but must be connected to the radiation source (which operates in the micron region) via the differentially pumped connection. This arrangement allows the gas load from the source to be evacuated to a tolerable pressure before it reaches the research chamber. No windows could be used to impede the gas flow, of course, due to the opacity of all solid materials in the vacuum ultraviolet region. As can be seen in Fig. 13, the differential pumping system involves the use of three pumping units in tandem.

1 Environmental Chamber System Construction

The principal design features of the system are depicted in Fig. 14. Details of this construction together with summary descriptions of component parts and associated equipment are given in the following sections.

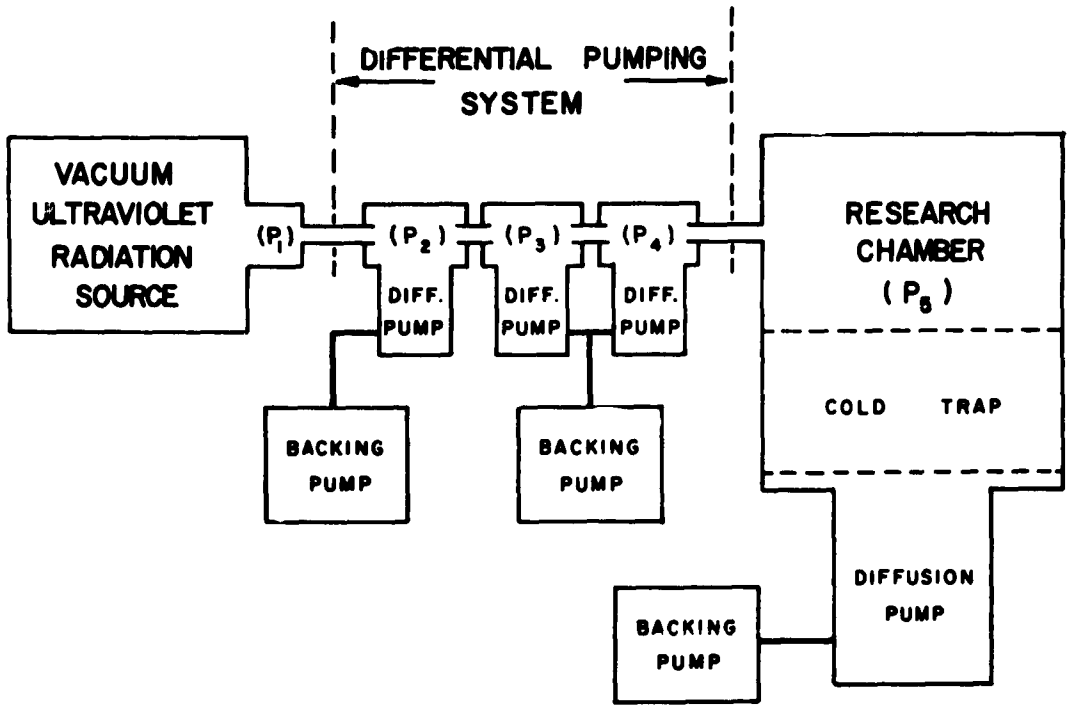

FIG. 13 SCHEMATIC ARRANGEMENT OF VACUUM ULTRAVIOLET RADIATION SOURCE AND ULTRA-HIGH VACUUM ENVIRONMENTAL CHAMBER SYSTEM

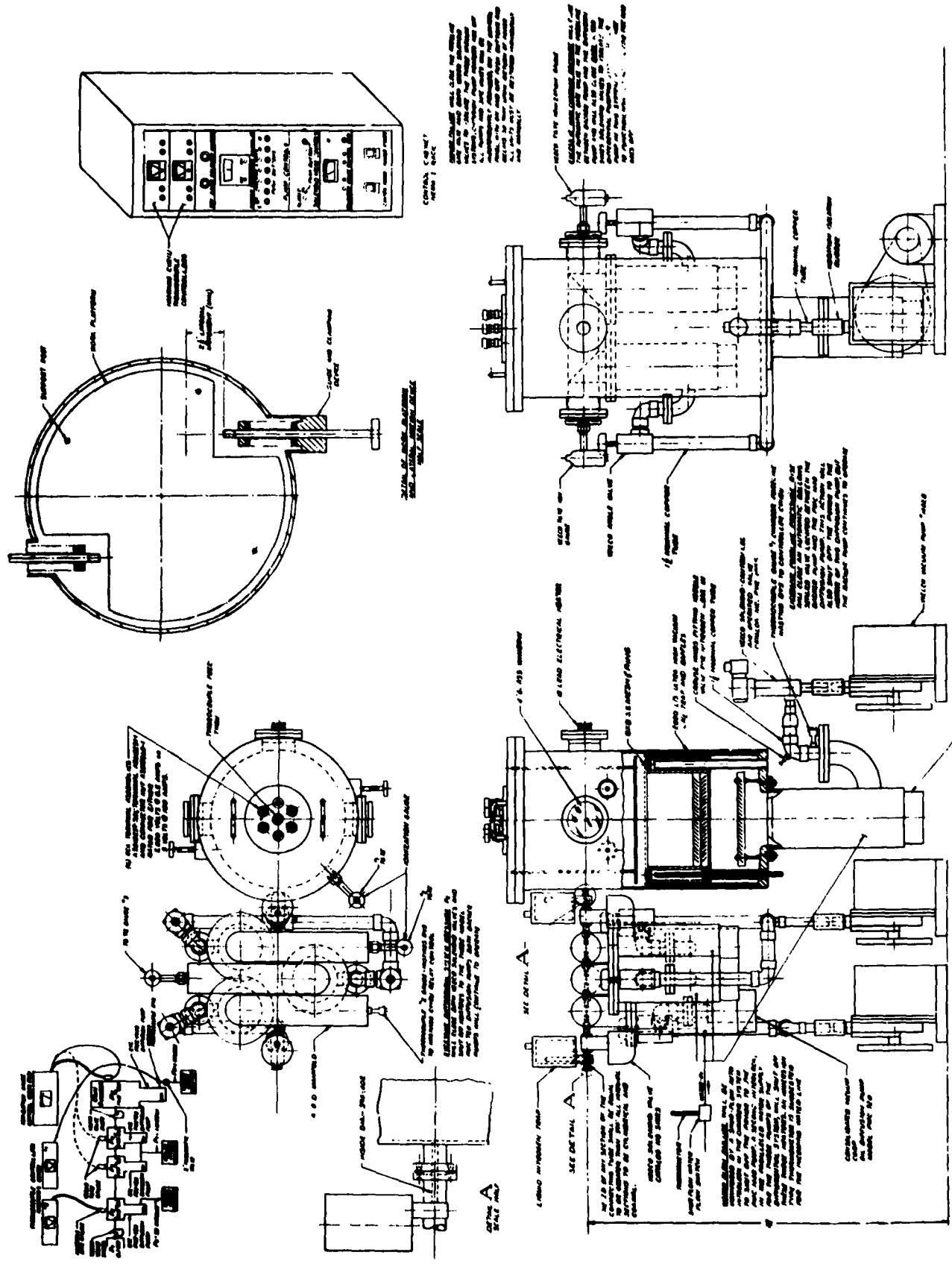

FIG. 14 PRINCIPAL DESIGN FEATURES OF ENVIRONMENTAL CHAMBER SYSTEM

1.1 Vacuum Chamber Fabrication

Stainless steel of the 304 series has been used throughout in the construction. This is evident in the interior view of the main chamber given in Fig. 15. The wall thickness of the main chamber is 0.250", while the differential chambers and manifolding are of standard 0.190" wall. All welds are full-penetration, fusion-arc welds of a high standard of quality, maintaining a clean, smooth finish of the chamber body. The cylindrical "work region" above the work platform suspended from the cover plate of the main chamber has the dimensions 18" diameter x 18" depth, with a resulting volume of 75 liters. All removable flanges on the main chamber use (double) crushable gold wire O-rings as vacuum seals.

1.2 Main Chamber Liquid Nitrogen Trap

This trap, enclosed within the chamber body, has a double diagonal-chevron baffle made from oxygen-free, high conductivity copper. The support tubing and antimigration shield is constructed of 304 stainless steel. The trap liquid nitrogen volume is approximately 7 liters and this amount of refrigerant will last eight hours, after which the trap very slowly warms up. Depending on the operating conditions, the trap is effective for total periods of 10-16 hours per filling. A secondary, single chevron baffle is placed directly over the chamber pump throat to collect pump condensates.

1.3 Main Chamber Diagnostic and Functional Equipment

The main chamber is equipped as follows:

(a) Two 4 inch diameter observation windows of polished Corning 7056 optical glass are so placed, 180° apart, as to permit wide angle observation of the work region without obstruction.

(b) An electrical feed-through header, with 22 feed-through wires, is placed in the chamber wall to provide service, e.g., the vacuum ultraviolet photomultiplier detector. The header is welded to a flange

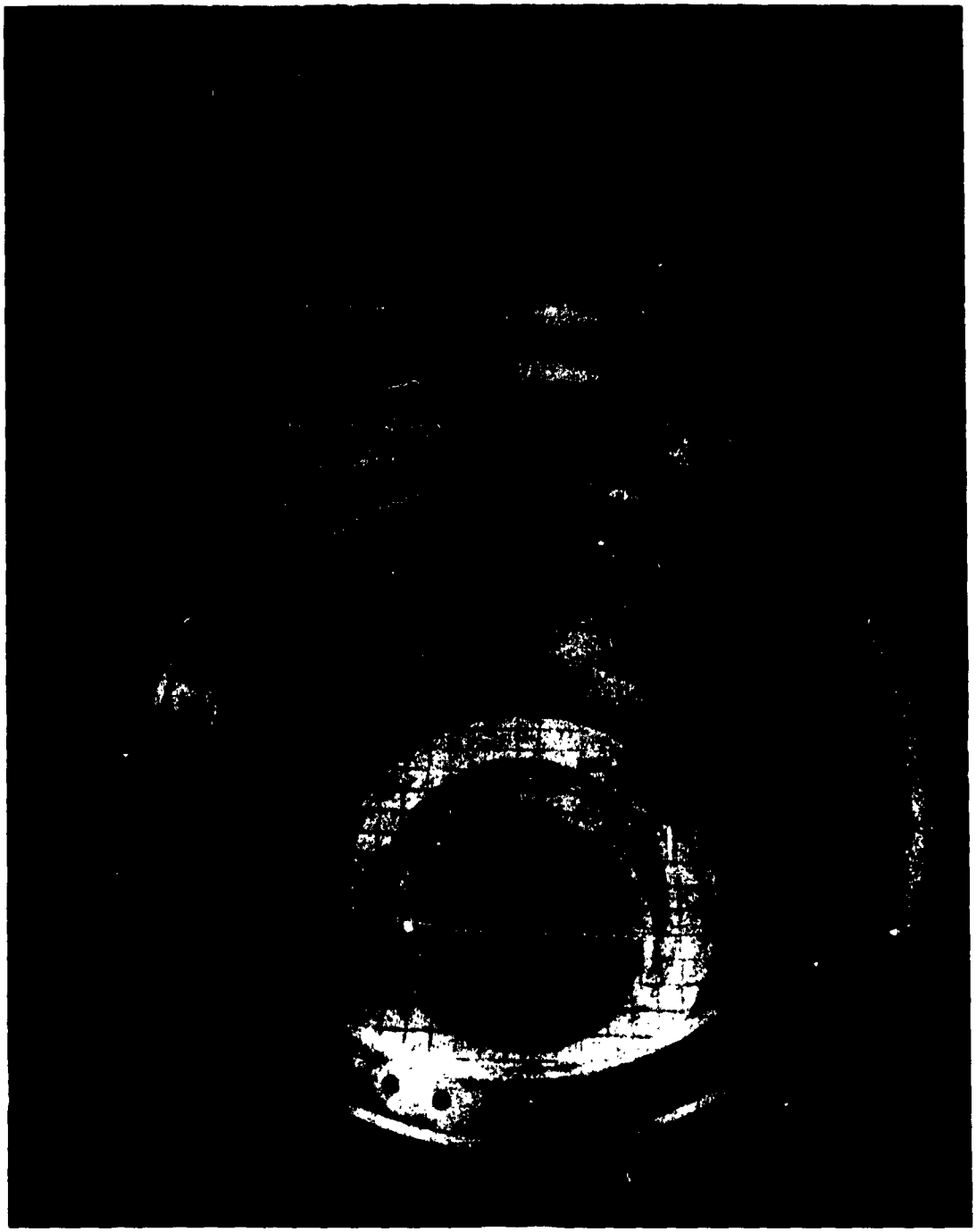

FIG. 15 INTERIOR VIEW OF THE SPACE ENVIRONMENTAL SIMULATION CHAMBER LOOKING TOWARDS THE VACUUM ULTRAVIOLET RADIATION SOURCE

mount and is positioned diametrically opposite the radiation source connection. The header and the two windows, mentioned above, are oriented 90° with respect to each other and are so designed as to be interchangeable.'

(c) A work support platform of stainless steel is suspended from the cover plate by four adjustable and removable stainless steel support rods. These are positioned to avoid interference with either the observation windows or the linear-motion devices.

(d) Two linear-motion devices each provide a minimum of 3 inches of lateral movement near the center of the chamber through a system of fusion-welded, flexible, stainless steel bellows. They can be positioned and locked by an external clamping device.

(e) A flange mounted electrical power feed-through array is centrally placed on the main chamber cover plate. The array consists of six Almanax insulated conductors rated for both 100 amperes at 5 volts AC, or 0.5 amperes at 2000 volts DC, together with a small header for 3 pairs of thermocouple leads.

(f) The chamber is fitted with a gold o-ring sealed flange which mates with another for attachment to the differentially pumped system. This flange is designed so as to permit removal of the differentially pumped connection and allow direct attachment of the radiation source.

(g) A glass enclosed Veeco RG-75 gauge tube is fitted to the chamber with stainless steel fittings attached to a Kovar ferrule sealed to the gauge.

(h) A purging valve, for admitting dry air or other gas to the main chamber, is situated between the chamber's diffusion and backing pumps.

2 Differential Pumping System Construction

This system, interposed between the radiation source and the research chamber, consists of three interconnected ballast tank sections, each with its own pumping unit. (See Fig. 15.) The sections have been so arranged as to place the associated 4 inch diffusion pumps in a compact, triangular cluster, resulting in an overall length of only 60 centimeters. The ballast tanks serve as expansion chambers for the pulsed gas load from the source.

The three ballast chambers are connected by open tubing of inside diameter equal to or greater than .394" (effective source aperture). This tubing is cylindrical and coaxial such that its axis is a line connecting the center of the radiation source to the center of the working region in the main chamber.

The extremities of the differential pumping system are each fitted with an optically open, finger type, liquid nitrogen cold trap. These traps prevent the diffusion pump oils in the differential system from migrating into the source or research chamber during source operation.

Referring to Figs. 13 and 14, chamber P_2, adjacent to the radiation source, is equipped with a Hastings type DV-5m thermocouple gauge giving pressure readings down to 1×10^{-4} mm Hg. Chambers P_3 and P_4 are equipped with Veeco RG-75 ionization gauge tubes installed in a similar way to the gauge on the main chamber.

3 Environmental System Pumps

Each section of the differential system is equipped with a Consolidated Vacuum Corporation (C.V.C.) Model PMC-720 oil diffusion pump. These diffusion pumps are backed by Welch 1402B mechanical pumps in the arrangements shown in Fig. 14. The main chamber is equipped with a C.V.C. Model PMC-1440 oil diffusion pump and is backed by a third Welch 1402B rotary pump. Diffusion pumps P_2 and P_3 have been supplied with Convoil 20 as the pumping fluid, whereas pumps P_4 and P_5 are equipped with Monsanto OS 124 oil.

4 Main Chamber Bake-Out System

The bake-out system will bake the main chamber (only) to 450°C, with removable blanket type heaters of Nichrome wire. These are clearly seen in Fig. 1. Individual heaters serve all diagnostic parts and the main chamber ionization gauge.

All heaters are arranged in a balanced three-phase system with a load of approximately 3.5 KW per phase. Temperature control and indication are interconnected to a panel on the control rack.

5 Fail-Safe Protection System

Fail-safe devices have been incorporated into the system to minimize damage in case of system malfunction. The following eventualities will activate the various components of the protective system:

a. Excessive foreline pressure

b. Excessive main chamber pressure

c. Excessive differential system pressure

d. Insufficient cooling water flow

e. Power failure.

The exact sequence of events for each of these eventualities is detailed in Fig. 14.

6 Performance of Vacuum System

Upon installation, the main chamber was baked out at 450°C and various tests made on the performance of the pumping units. The capability indicated by these tests has been subsequently verified on several occasions.

Following bake-out, the main chamber pumps down to a pressure of 1×10^{-9} mm Hg. Pressures of this order have been reached even after the chamber has been opened to the atmosphere several times over a period of eight weeks after bake-out. This means, of course, that materials with temperature sensitive properties need not be subjected to high (up to 450°C) bake-out temperatures in order to be tested at pressures of order 10^{-9} mm Hg.

Only two hours are required to reduce the main chamber pressure to the low 10^{-8} mm Hg. region. From this point overnight

pumping (24 hours maximum) is necessary to reach the low 10^{-9} mm Hg. region.

Referring to Fig. 13, the pressures given in the left hand column of Table 1 are those typically obtained during system operation when the radiation source is valved off from the differential connection. The pressures in the right hand column of the table are typically obtained with the source open to the main chamber through the differential system. The source was operated by the gas pulsing technique, the pressures listed being the peak gauge readings observed. Even at the highest pulse rate of one per second, the main chamber pressure remains on the 10^{-9} mm Hg. scale.

TABLE 1

VACUUM SYSTEM OPERATIONAL PRESSURES

Pressure, mm Hg.	Source Valved	Source Open
P_1	--	10^{-1}
P_2	$< 10^{-4}$ *	$< 10^{-4}$ *
P_3	2×10^{-6}	3.5×10^{-6}
P_4	1×10^{-6}	1.1×10^{-6}
P_5	1.5×10^{-9}	5×10^{-9}

* Lower limit of gauge

V. PHOTOMULTIPLIER DETECTOR EVALUATION OF RADIATION PULSE

The open photomultiplier is mounted in the environmental chamber such that its cathode is directly opposite and aligned with the exit aperture of the pulsed radiation source. This will be understood by comparison of Figs. 15 and 17. This arrangement places the photocathode in immediate proximity to the position where material samples are held during irradiation in the chamber. The intensity of radiation determined by the detector is, accordingly, a sufficiently accurate measure of the radiation falling on a test sample.

After the source and detector were sealed to the environmental chamber, the latter was evacuated and detector evaluation of the radiation source output performed. A typical response of the detector to a pulse of radiation is shown in Fig. 16 A. The pulse shapes reproduced in this figure were recorded on a Hughes Model 105 Memoscope connected in the detector circuit. The horizontal scale represents 100 microseconds per division while the vertical scale is 50 volts per division. The high voltage applied to the photomultiplier was 3700 volts while the radiation source was operated at 10 kV. Figure 16A actually shows 2 source pulses fired successively. their similarity being an indication of source stability. The recorded pulse length is seen to be less than 1 millisecond. For operation of the detector integrator, the time constant of the circuit must be large compared to the pulse duration. It was for this purpose, as explained in part 2.1 of Section III and shown in Fig. 12, that the 10^5 ohm resistor was placed in series with the integrator diode.

The pulse shapes reproduced as Figs. 16B, C, and D were recorded with filters of lithium fluoride, quartz, and flint glass interposed between the detector and source aperture, the source voltage being

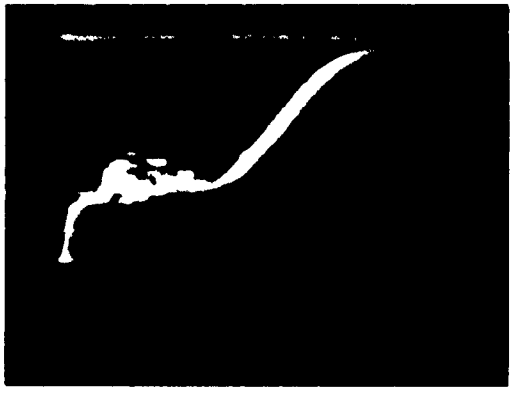

A. Unfiltered Pulse

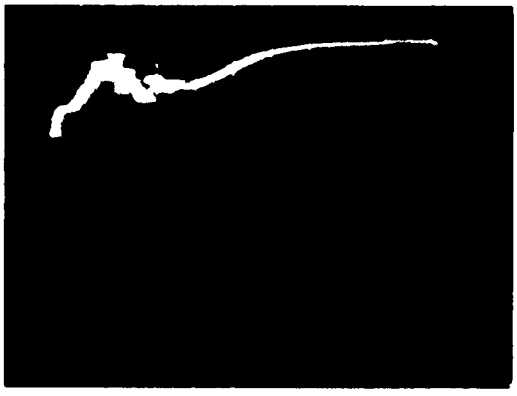

B. Lithium Fluoride Filter

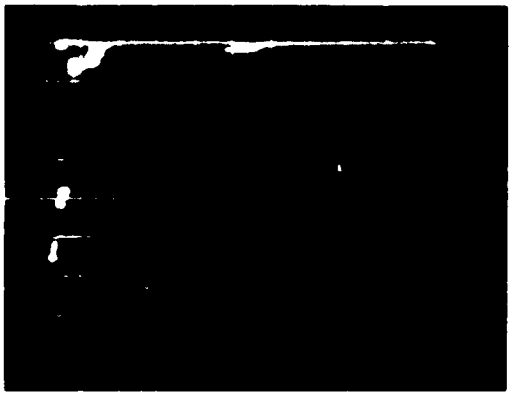

C. Quartz Filter

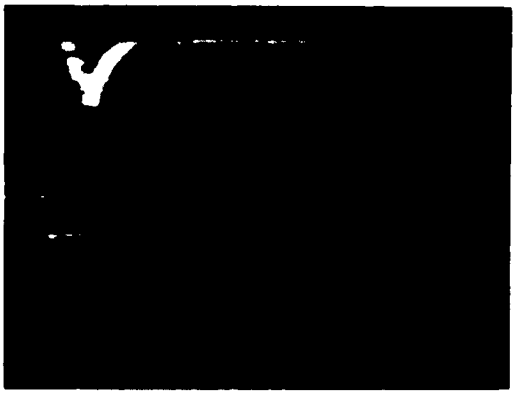

D. Flint Glass Filter

Horizontal scale: 100 μ sec/div

Vertical scale: 50 volts/div

FIG. 16 MEMOSCOPE TRACES OF THE PHOTOMULTIPLIER DETECTOR RESPONSE TO A 10 kv RADIATION PULSE WITH VARIOUS FILTERS IN BEAM.

10 kV in all cases. The fact that a small response was recorded with a flint glass filter (short wavelength cut-off at about λ3000) although the detector threshold is at about λ2500 was due to scattered radiation in the chamber reaching the detector. Comparison of Figs. 16A and B indicates that a good proportion of the radiant energy in a pulse lies below λ1100, the short wavelength cut-off of the lithium fluoride filter.

Verification of the satisfactory operation of the integrator was obtained during this series of observations by comparing the relative magnitudes of the areas under the various pulse curves recorded with the corresponding values of the integrator voltage meter.

1 Measurement of the Radiation Pulse Energy

To evaluate the relationship between the integrator response and the actual radiant energy per pulse incident on the detector, consider a band of wavelengths, $\Delta\lambda$, centered around λ. Then, if $\Delta\mathcal{J}(\lambda)$ is the intensity of this bandwidth,

$$\Delta\mathcal{J}(\lambda) = \frac{\Delta N(\lambda) hc}{A\,\lambda} \tag{1}$$

where, $\Delta N(\lambda)$ is the number of photons per second of this band incident upon the detector and is, in general, a function of λ,

A is the area of the detector,

h is Planck's constant, and

c is the velocity of light.

Now by definition,

$$Q(\lambda) \equiv \frac{\Delta n\,(\lambda)}{\Delta N\,(\lambda)} \tag{2}$$

where, $Q(\lambda)$ is the quantum yield of the photocathode and

$\Delta n(\lambda)$ is the number of photoelectrons emitted/second.

Solving for $\Delta N(\lambda)$ in equation (1) and substituting into equation (2) yields:

$$Q(\lambda) = \frac{\Delta n(\lambda) hc}{A\,\lambda\,\Delta\mathcal{J}(\lambda)} . \tag{3}$$

Remembering that $\Delta n(\lambda) = \frac{\Delta I_K(\lambda)}{e}$, where $\Delta I_K(\lambda)$ is the cathode emission current corresponding to the bandwidth $\Delta\lambda$, and e is the electronic charge, one can solve equation (3) for $\Delta I_K(\lambda)$, giving:

$$\Delta I_K(\lambda) = \left(\frac{e A}{h c}\right) \lambda Q(\lambda) \Delta \mathcal{I}(\lambda)$$

$$= \left(\frac{e A}{h c}\right) \lambda Q(\lambda) \frac{\Delta \mathcal{I}(\lambda)}{\Delta \lambda} \Delta \lambda \qquad (4)$$

In the limit when $\Delta\lambda \to o$,

$$dI_K = \left(\frac{e A}{h c}\right) \lambda Q(\lambda) \mathcal{I}'(\lambda) \, d\lambda$$

where, $\mathcal{I}'(\lambda) = \frac{d\mathcal{I}(\lambda)}{d\lambda}$ is the intensity per unit wavelength, and

$$I_K = \frac{e A}{h c} \int_{\lambda_2}^{\lambda_1} \lambda Q(\lambda) \mathcal{I}'(\lambda) \, d\lambda \qquad (5)$$

where I_K is the cathode current corresponding to the over-all spectrum.

The relationship of equation (5) is actually an implicit one in that what is required is $\mathcal{I}'(\lambda)$ from which the total intensity, and thence the energy in a pulse, can be deduced. However, this would involve a knowledge of ΔI_K as a function of λ, i.e., wavelength scanning of the radiation pulse. Since this is not possible in the system being described, it was decided to use the relationship between the corresponding variables in the form of equation (5) and to deduce the answer by approximation. The simplest approach is, of course, to assume all variables constant. Walker, et.al. (Ref. 1) have measured the quantum yield of nickel in the wavelength range $\lambda\lambda$1400-500 and have found the values, for a particular heat treatment, to lie in the vicinity of 0.02 electrons per photon. Above λ1400, the yield is of the order of 10^{-3} electrons per photon. Other data on nickel by Lukirskii, et al., (Ref. 2) range from 0.02 at λ23.6 to 0.05 electrons

per photon at λ113. If the further assumption is made that the source output is flat from λ50 to λ2500 (the long wavelength cut-off of the nickel cathode), then equation (5) can readily be evaluated in terms of $\mathcal{J}'$.

$$\text{Let } Q(\lambda) = \begin{cases} 2 \times 10^{-2} & \text{for } \lambda < \lambda_\alpha \\ 10^{-3} & \text{for } \lambda > \lambda_\alpha \end{cases}$$

where λ_α is taken as 1400 Å. Then, equation (5) gives:

$$I_K = \frac{e\,A}{2hc} \mathcal{J}' \left[(2 \times 10^{-2})(\lambda_\alpha^2 - \lambda_1^2) + 10^{-3}(\lambda_2^2 - \lambda_\alpha^2) \right]$$

$$\text{and } \mathcal{J}' = \frac{2hc\ I_K}{e\,A \left[(2 \times 10^{-2})(\lambda_\alpha^2 - \lambda_1^2) + 10^{-3}(\lambda_2^2 - \lambda_\alpha^2) \right]} \quad (6)$$

The cathode current can be expressed in terms of the plate output voltage by:

$$I_K = \frac{V_A}{R_L G} \quad (7)$$

where, V_A is the anode output voltage,
R_L is the plate load resistor, and
G is the gain of the photomultiplier.

Remembering that $\mathcal{J}'$ and V_A are both functions of time, t, substitution of equation (7) in (6) yields:

$$\mathcal{J}'(t) = \frac{2hc}{eAR_L G} \frac{V_A(t)}{(2 \times 10^{-2})(\lambda_\alpha^2 - \lambda_1^2) + 10^{-3}(\lambda_2^2 - \lambda_\alpha^2)} \quad (8)$$

Finally, the energy in a pulse per unit wavelength (E') is evaluated by integrating equation (8) over the duration of the pulse; i.e.,

$$E' = A \int \mathcal{J}' \, dt = \frac{2\,hc}{eR_L G} \frac{\int V_A(t)\ dt}{(2 \times 10^{-2})(\lambda_\alpha^2 - \lambda_1^2) + 10^{-3}(\lambda_2^2 - \lambda_\alpha^2)}$$

$$= \frac{2\,hc\,T}{e\,R_L G} \frac{V_C}{(2 \times 10^{-2})(\lambda_\alpha^2 - \lambda_1^2) + 10^{-3}(\lambda_2^2 - \lambda_\alpha^2)} \quad (9)$$

where, T is the time constant of the integrator, and

V_C is the integrator output voltage.

Equation (9) gives the energy per unit wavelength in a pulse of radiation in terms of the integrator response. Thus, in the case of the 10 kV pulse shown in Fig. 16A, the integrator response was 1.28 volts. On substituting appropriate values into equation (9), the value $E^{\dagger} = 7.40 \times 10^{-6}$ ergs/Å is obtained. Since the extent of the detectable spectrum is λλ 0-2500, this means that the total radiant energy in a 10 kV pulse, at the detector, is 0.02 ergs.

To investigate the maximum intensity of this pulse, equation (8) (where $V_A(t)$) refers to the peak anode voltage) can be used. With reference to Fig. 16A, the maximum value of V_A is approximately 200 volts while the cathode area is about 1 cm^2. The corresponding peak intensity is 1.15×10^{-2} ergs/cm^2/sec/Å. For the complete band the peak intensity is, accordingly, about 30 ergs/cm^2/sec.

As a check on the assumption that the source output is flat, a set of integrator readings obtained with and without the lithium fluoride filter (LiF) can be used. The short wavelength cut-off of LiF is around λ1100. Applying equation (9), in the case of the filtered pulse, gives:

$$E^{\dagger}(\text{LiF}) = \frac{2hc\,T}{e\,R_L\,G} \quad \frac{V_C\ (\text{LiF})}{\left(2 \times 10^{-2}\right)\left[\lambda_\alpha^{\,2} - \lambda_\beta^{\,2}\right] + 10^{-3}\left[\lambda_2^{\,2} - \lambda_1^{\,2}\right]} \qquad (10)$$

where λ_β is the LiF cut-off wavelength.

Dividing equation (9) by (10), yields:

$$\frac{E^{\dagger}(\text{total})}{E^{\dagger}(\text{LiF})} = \frac{V_C\ (\text{total})}{V_C\ (\text{LiF})} \left[\frac{2 \times 10^{-2}\left(\lambda_\alpha^{\,2} - \lambda_\beta^{\,2}\right) + 10^{-3}\left(\lambda_2^{\,2} - \lambda_1^{\,2}\right)}{2 \times 10^{-2}\left(\lambda_\alpha^{\,2} - \lambda_1^{\,2}\right) + 10^{-3}\left(\lambda_2^{\,2} - \lambda_1^{\,2}\right)}\right] \qquad (11)$$

which, on substituting appropriate values, and with V_C (LiF) = 0.30 volts, gives that

$$\frac{E^{\dagger}(\text{total})}{E^{\dagger}(\text{LiF})} \simeq 1.5.$$

The assumption of a flat source output is equivalent to $E^{\dagger}$ having a constant value. If this were exactly true, the above ratio would be unity. The fact that its value is actually close to 1.5 means that the average value of the energy per unit wavelength over the complete spectrum is 50 percent larger than the average value for wavelengths $> \lambda 1100$.

VI. THE EFFECTS OF VACUUM ULTRAVIOLET RADIATION AND/OR ULTRAHIGH VACUUM ON A SILICON SOLAR CELL

The purpose of this experiment was to investigate whether the characteristic voltage-current curve of a silicon solar cell was affected by exposure of the cell to vacuum ultraviolet radiation and/or an ultrahigh vacuum.

The experimental arrangement is depicted in Figs. 17 and 18. Two 10 percent efficient gridded cells (Hoffman Electronics Company) of dimensions 1 x 2 cm were mounted vertically on two adjacent faces of a square copper block. The cells were soldered by their tinned backs to the block which was attached to an extension of one of the mechanical motion devices. The block thus effectively acted as a common negative terminal for the cells, the grounded electrical connection to which was made through a copper wire spring attached to one of the feedthroughs in the chamber cover plate. Similarly, two other copper springs were used to make electrical connections to the positive contact grids on the front surfaces of the cells.

The copper block was oriented such that both cells could be illuminated with visible and near infrared light from a 100 watt concentrated zirconium arc source (George W. Gates Company, Type G157). When thus illuminated the characteristic curves of either cell could be determined from measurements made with the circuit shown in Fig. 19. The collimated beam from the arc source entered the chamber through one of its window ports, and that portion not intercepted by the solar cells passed out of the chamber through the opposite window where its intensity was monitored with an Eppley thermopile. The thermopile read-out was by means of a Leeds and Northrup galvanometer.

FIG. 17 INTERIOR VIEW OF ENVIRONMENTAL CHAMBER SHOWING SOLAR CELL EXPERIMENTAL ARRANGEMENT. The cell mounting block is seen directly in front of the photomultiplier structure

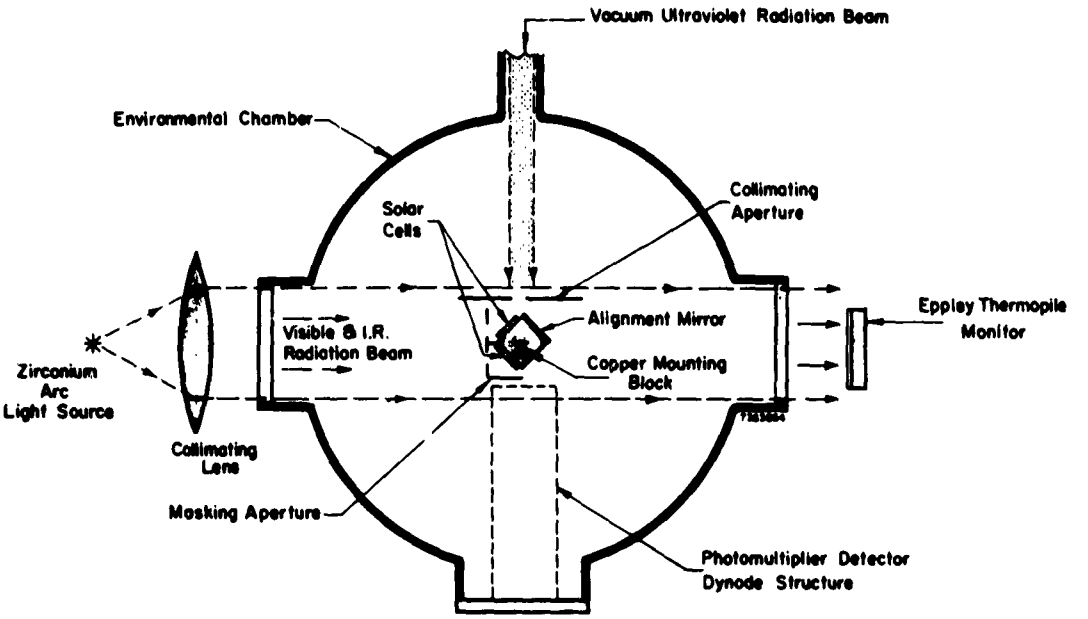

FIG. 18 SCHEMATIC CROSS SECTION OF THE SILICON SOLAR CELL EXPERIMENTAL ARRANGEMENT

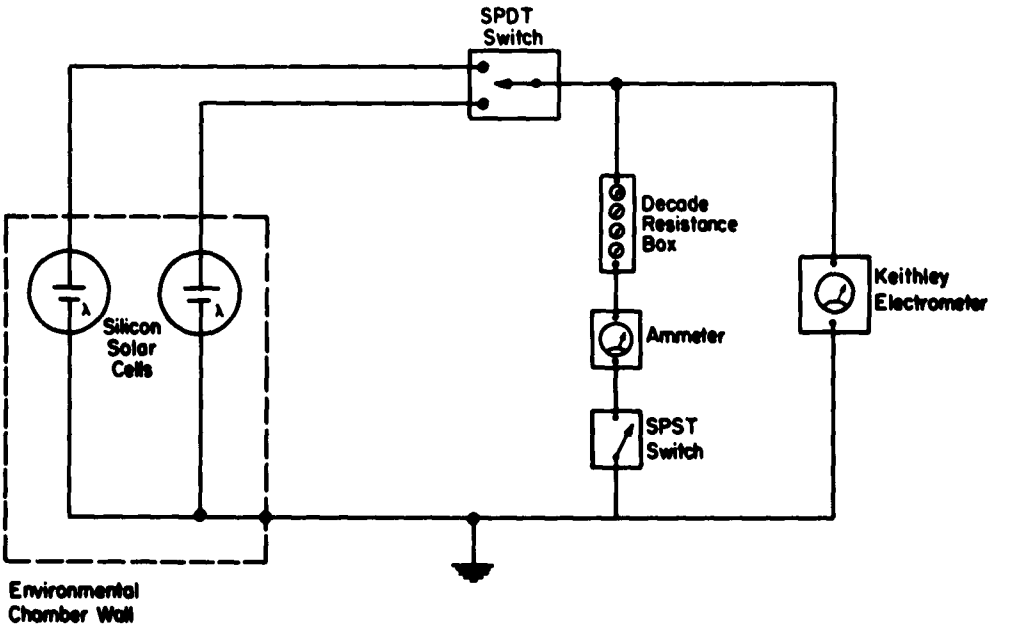

FIG. 19 SCHEMATIC DIAGRAM OF THE ELECTRICAL CIRCUIT USED IN THE DETERMINATION OF CHARACTERISTIC CURVES OF SILICON SOLAR CELLS

With the copper block correctly positioned by means of the mechanical motion device one of the cells was opposite the vacuum ultraviolet source aperture and could be irradiated. The second (monitor) cell was shielded from the radiation and hence was exposed to the vacuum only. A small mirror attached to one of the back faces of the mounting block facilitated its alignment.

1 Experimental Results

The effect of vacuum alone on the solar cell which was not irradiated is shown by the characteristic curves presented in Fig. 20. One curve was plotted from current and voltage readings taken with the chamber at atmospheric pressure, while the second curve corresponds to a chamber pressure of 10^{-8} mm Hg. The intensity of illumination of the cell by the arc source was monitored with the thermopile during the measurements and found to be sufficiently constant.

It is evident from the curves of Fig. 20 that the cell response is strongly affected by the degree of vacuum it experiences. Since the power generated by the cell is greater when illuminated at reduced pressure it is possible that the effect is due to removal of contaminating surface layers which would otherwise absorb, or even enhance reflection of, some of the incident energy.

The possible effect of vacuum ultraviolet radiation on the performance of a solar cell was investigated by subjecting the cell mounted opposite the source aperture to 100 pulses of 10 kv radiation. The chamber pressure during this experiment was about 3×10^{-9} mm Hg. Prior to the irradiation both cells were illuminated with the arc light source and their characteristic curves plotted as shown in Fig. 21. This figure also shows the characteristic curves obtained for both cells after the one noted had been irradiated. The thermopile monitor indicated that the intensity of illumination on the cells did not change significantly during the characteristic measurements.

A comparison of the pairs of curves given in Fig. 21 for the irradiated and non-irradiated cells respectively indicates a

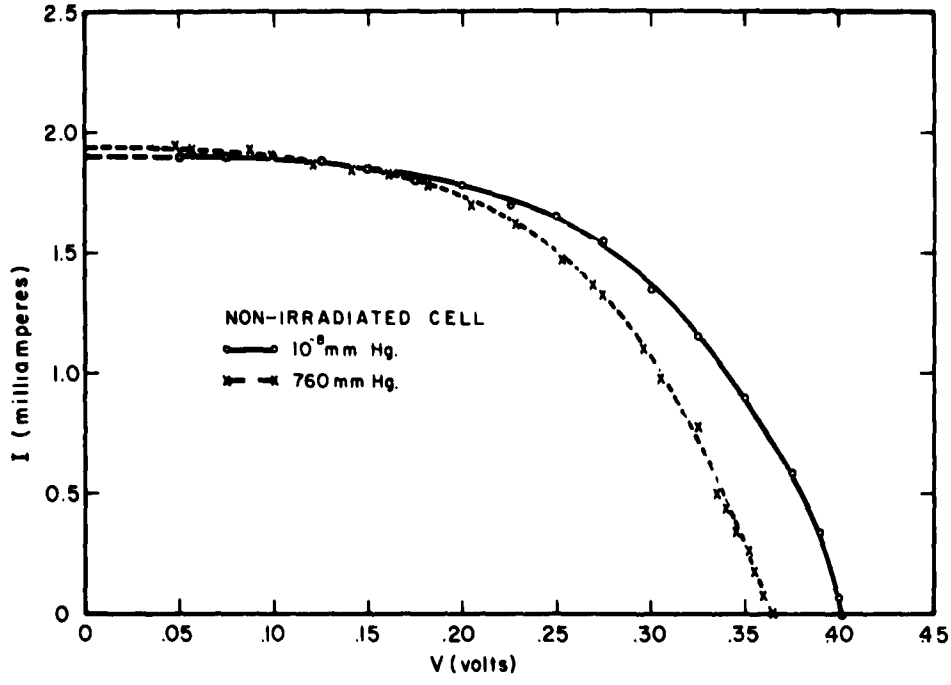

FIG. 20 THE EFFECT OF ULTRA-HIGH VACUUM ON THE CHARACTERISTIC CURVE OF A SILICON SOLAR CELL

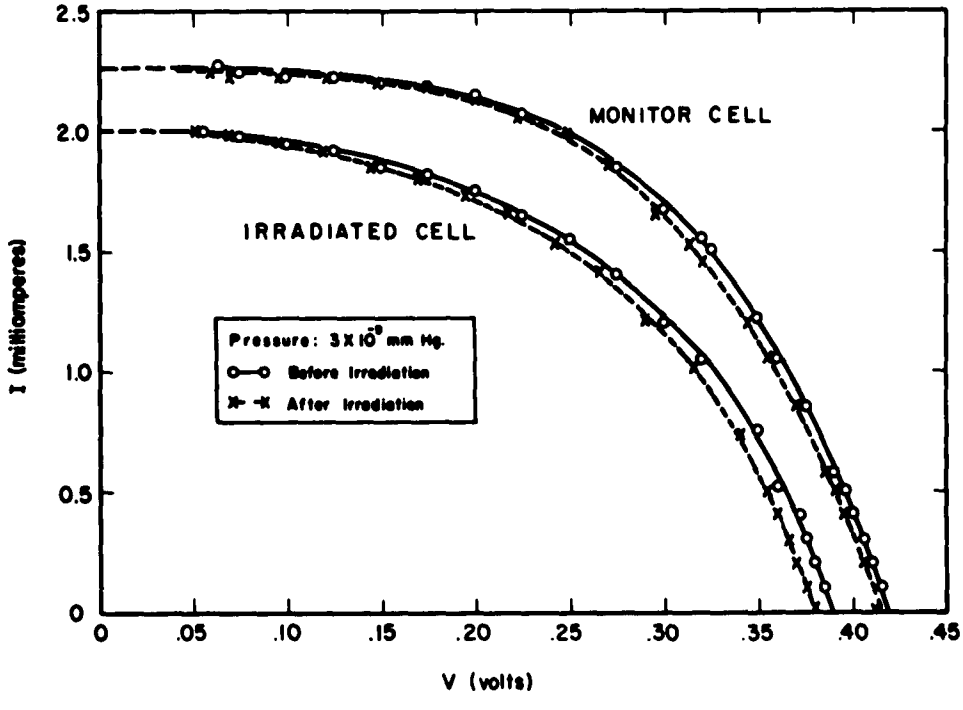

FIG. 21 THE EFFECT OF VACUUM ULTRAVIOLET RADIATION ON THE CHARACTERISTIC CURVE OF A SILICON SOLAR CELL

slightly greater separation in the former case. A priori, the two curves for the non-irradiated (monitor) cell would be expected to coincide, since they were recorded for essentially identical conditions. The fact that they do not, cannot be explained on the basis of the available data and, accordingly, makes it impossible to draw a definite conclusion as to whether the vacuum ultraviolet radiation did affect the irradiated cell.

VII. THE EFFECTS OF VACUUM ULTRAVIOLET RADIATION AND/OR ULTRAHIGH VACUUM ON THE OPTICAL REFLECTANCE OF METALLIC MIRROR COATINGS

This experiment consisted of preparing several metal mirrors by vacuum evaporation and measuring their spectral normal specular reflectances*, both before and after exposure to radiation and/or ultrahigh vacuum in the environmental chamber.

Four sets of mirrors were prepared, each set consisting of three mirrors made simultaneously and, therefore, under identical vacuum coating conditions. Each metal was evaporated from a tungsten filament onto an optically polished 2" x 2" BSC2 glass substrate to an opaque thickness, the coating chamber pressure being 10^{-4} mm Hg. Two metals with good visible reflectance were used in the fabrication of the test mirrors, viz., copper and gold. Gold was chosen as being chemically inert and copper as being, relatively, chemically active. Two of the sets of mirrors were prepared with a SiO protective overcoat which was deposited directly onto the metals without breaking vacuum. The other two sets were prepared with no overcoat. SiO overcoating (transparent to visible light) is used extensively for the protection of mirrored surfaces from chemical reactions, such as oxidation, when a mirror is exposed to air or a damaging atmosphere. Multilayer coatings of this type are also used in the spectral control of reflectances from optical surfaces. In view of these various applications, it was decided to test the copper and gold mirrors in both the coated and uncoated condition.

The reflectances of all mirrors were obtained with the aid of a Perkin-Elmer Model 13 U Spectrophotometer. The reflectance spectrum for each mirror was measured in the range λλ4000-6500, this being considered sufficient for the purpose of determining any change in

---

* 'Spectral normal specular reflectance' is referred to hereinafter as simply 'reflectance'.

reflectance as a result of the effect of the environment. Following the reflectance measurements, two mirrors from each set were mounted inside the environmental chamber. The remaining mirror from each set of three was kept to act as a monitor or standard to which the other mirrors could be compared (via the spectrophotometer) after the environmental exposure. Of the two mirrors inside the vacuum chamber, one was mounted so that radiation from the source did not reach it. The other was mounted in a holder attached to one of the linear motion devices such that it could be positioned directly in the path of the radiation. In total then, four sets of two identical mirrors, half of which were to receive radiation-plus-vacuum and the other half to receive vacuum only, were mounted inside the environmental chamber.

After approximately the full day's time required to seal the system for operation at ultrahigh vacuum, the research chamber was evacuated to a pressure of order 10^{-9} mm Hg and allowed to remain in that condition for a period of approximately 72 hours before the irradiation of the mirrors commenced.

Each mirror was irradiated with 100 pulses of vacuum ultraviolet radiation from the discharge source. The operating voltage of the source was 15 kV and the pulse rate was approximately 5 per minute. Initially, a pulsing voltage of 20 kV was used but, after a short time, red hot particles were noticed impinging on the irradiated mirror with each pulse of radiation. Presumably the particles were being ejected from the surface of the molybdenum electrodes of the source as they heated up. In order to reduce the discharge current density to a value at which the electrode material did not melt, the source operating voltage was immediately reduced from 20 kV to a value of 14 kV. This allowed satisfactory operation at a pulse rate of 5 per minute, for a period of about 60 minutes, after which the particles again appeared, in a sporadic fashion. In an attempt to keep the radiation intensity at as high a level as possible, the voltage was not further reduced. Instead, the pulse rate was immediately decreased whereupon there was no further ejection of particles from the source.

The pressure readings in the research chamber were monitored during the operation of the radiation source and at no time did the chamber ionization gauge register a pressure greater than 8×10^{-9} mm Hg. Generally, the pressure rose from about 2×10^{-9} mm Hg. to about 5×10^{-9} mm Hg. during the source discharge.

1 Experimental Results

Upon removal of the mirrors from the environmental chamber, their reflectances (together with those of the monitor mirrors) were re-measured on the spectrophotometer. Each reading was taken three times and the average values recorded. This was done to reduce the influence of instrumental fluctuations, the resulting possible error being less than ±3 percent.

The re-measured reflectance values are compared in Figs. 22, 23, 24, and 25 with those obtained before the mirrors were exposed to the chamber environment. The comparison is made by plotting reflectance change for each mirror as a function of wavelength. Examination of the depicted results indicates that a significant reflectance change appears to have occurred for the Cu + SiO mirror exposed to vacuum only (Fig.25) and also for the Cu mirror exposed to vacuum only (Fig. 24). In both cases the reflectance change is greatest at the short wavelength end of the measured range λλ4000-6500.

That the vacuum alone, rather than the combined effects of vacuum and radiation, would cause a reflectance change was not expected. Since the reflectance changes observed appeared greatest at the shortest reflected wavelengths, it was decided to repeat the reflectance measurements at the shortest wavelength covered by the spectrophotometer, viz., λ2500. Since no measurements were taken at λ2500 before the environmental exposure, a strict before-after comparison cannot be made. However, a valid comparison can be made with the monitor mirror if it is assumed not to have changed significantly during the course of the experiment, and if the other mirrors in the same set as the monitor had the same reflectance at all wavelengths before the

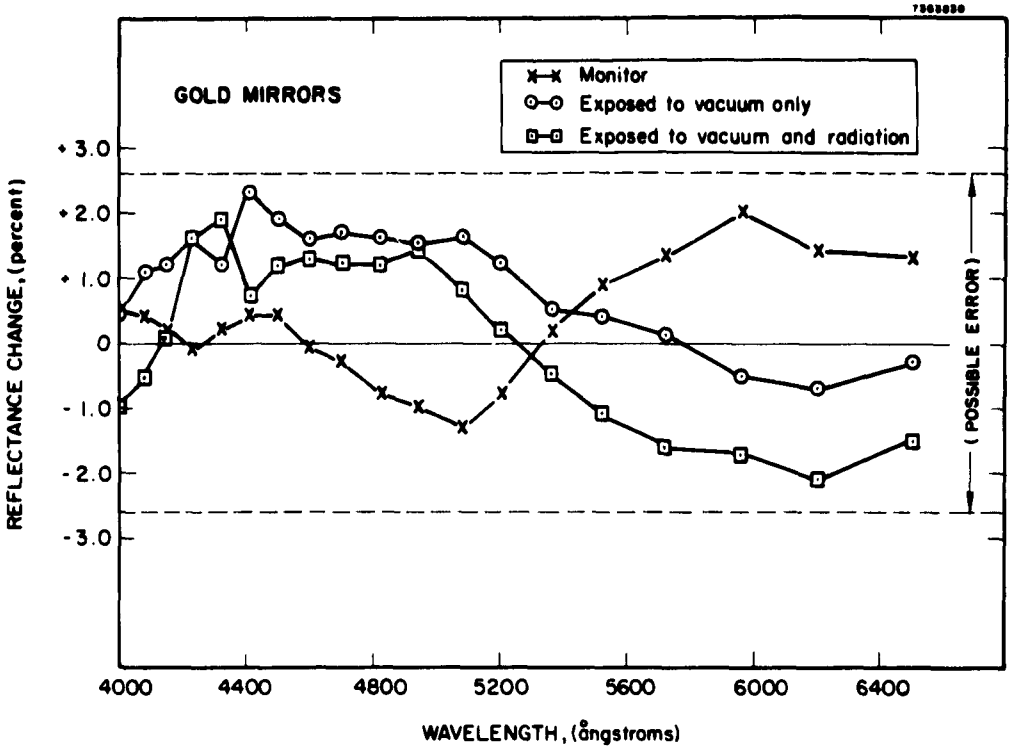

FIG. 22 THE EFFECT OF ULTRA-HIGH VACUUM AND/OR VACUUM ULTRAVIOLET RADIATION ON THE OPTICAL REFLECTANCE OF A GOLD MIRROR

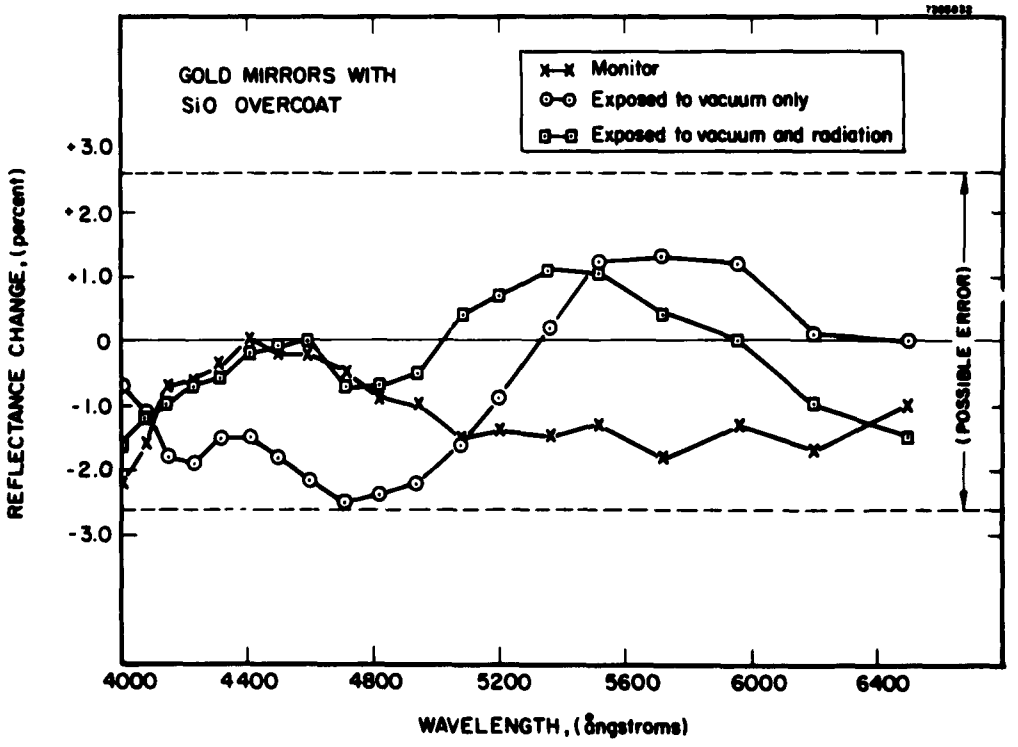

FIG. 23 THE EFFECT OF ULTRA-HIGH VACUUM AND/OR VACUUM ULTRAVIOLET RADIATION ON THE OPTICAL REFLECTANCE OF A SILICON MONOXIDE OVERCOATED GOLD MIRROR

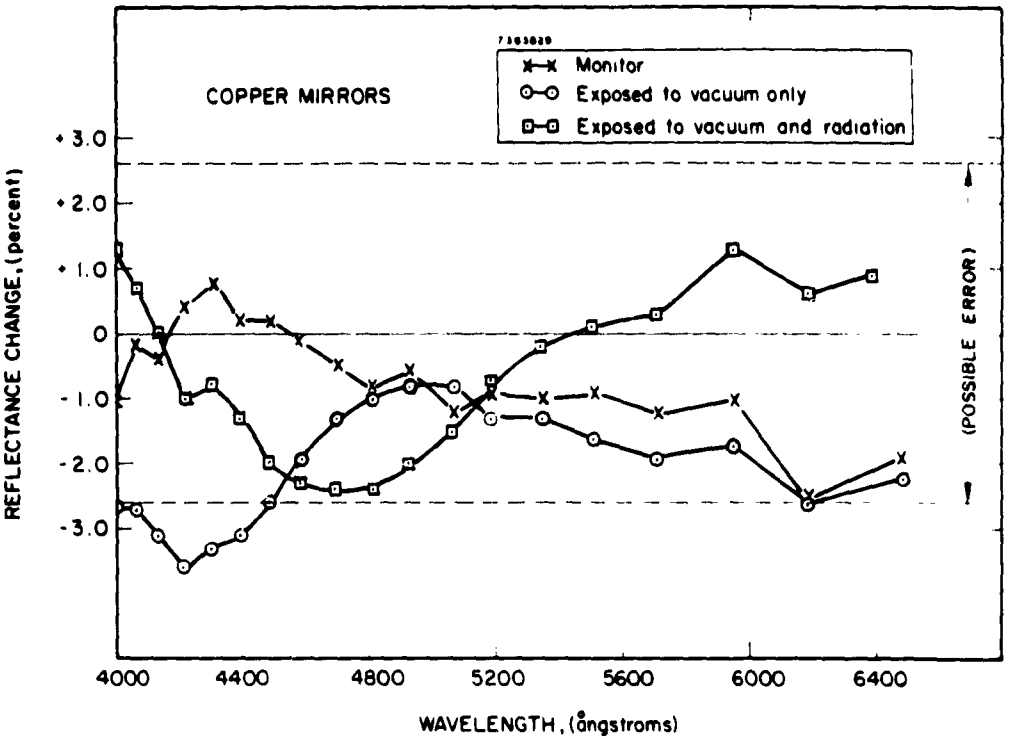

FIG. 24 THE EFFECT OF ULTRA-HIGH VACUUM AND/OR VACUUM ULTRAVIOLET RADIATION ON THE OPTICAL REFLECTANCE OF A COPPER MIRROR

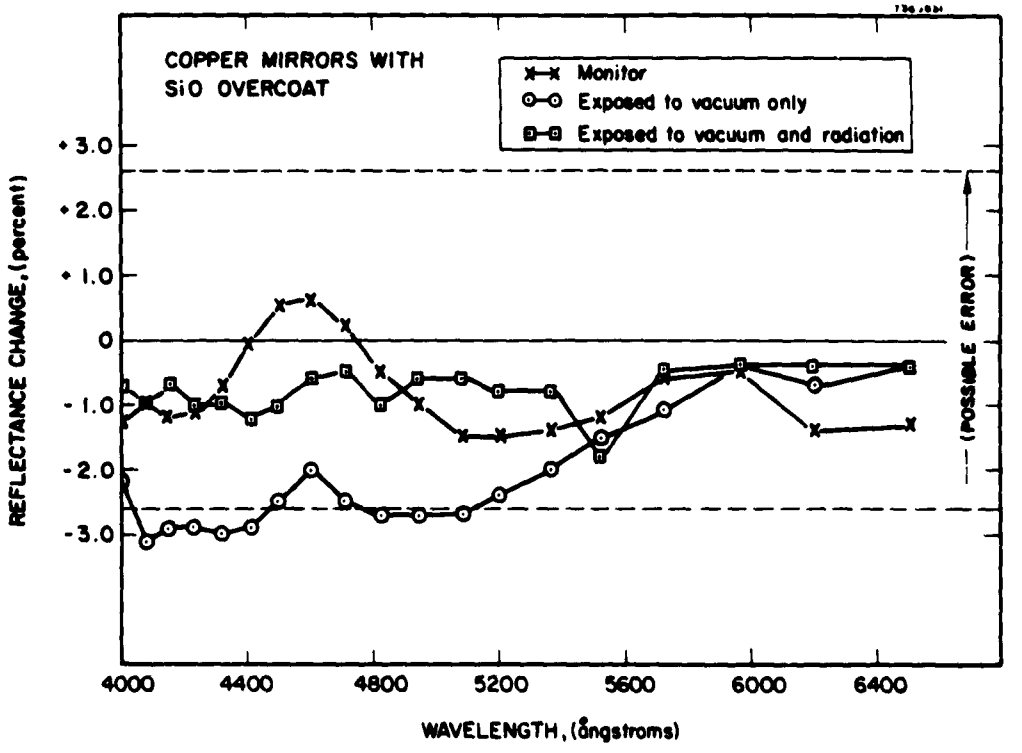

FIG. 25 THE EFFECT OF ULTRA-HIGH VACUUM AND/OR VACUUM ULTRAVIOLET RADIATION ON THE OPTICAL REFLECTANCE OF A SILICON MONOXIDE OVERCOATED COPPER MIRROR

environmental exposure. The justification for this assumption lies in the fact that the mirrors of each set were made under identical evaporating conditions. Measurements of the reflectances in the range λλ4000-6500 have borne out this assumption to within the experimental accuracy of the spectrophotometer.

The reflectance changes found at λ2500, by comparing the measured reflectance of each mirror in a set to the monitor of that set, are shown in Fig. 26. It is seen that significant reflectance changes occur for all the overcoated mirrors, whereas the uncoated surfaces show no significant change in reflectance as a result of the environmental exposure. Further, in the case of the overcoated mirrors, the reflectance decrease due to exposure to ultrahigh vacuum alone is greater than the decrease due to the combined effects of radiation and vacuum. It is also pertinent to note that the ratio of change due to vacuum to the change due to vacuum plus radiation is constant for both the gold and copper mirror sets with the SiO overcoating.

Given the validity of the results depicted in Fig. 26 the conclusion must be drawn that the optical reflectance of the silicon monoxide overcoated metallic mirrors deteriorated due to the ultrahigh vacuum exposure. Since the same vacuum condition was experienced by the irradiated mirrors, the further conclusion can be drawn that the radiation had an inhibiting effect on the mirror deterioration. The fact that the measurements on the plain metal mirrors evidence no reflectance change of significance indicates that the overcoated mirror deterioration results from changes in the optical characteristics of the overcoating material.

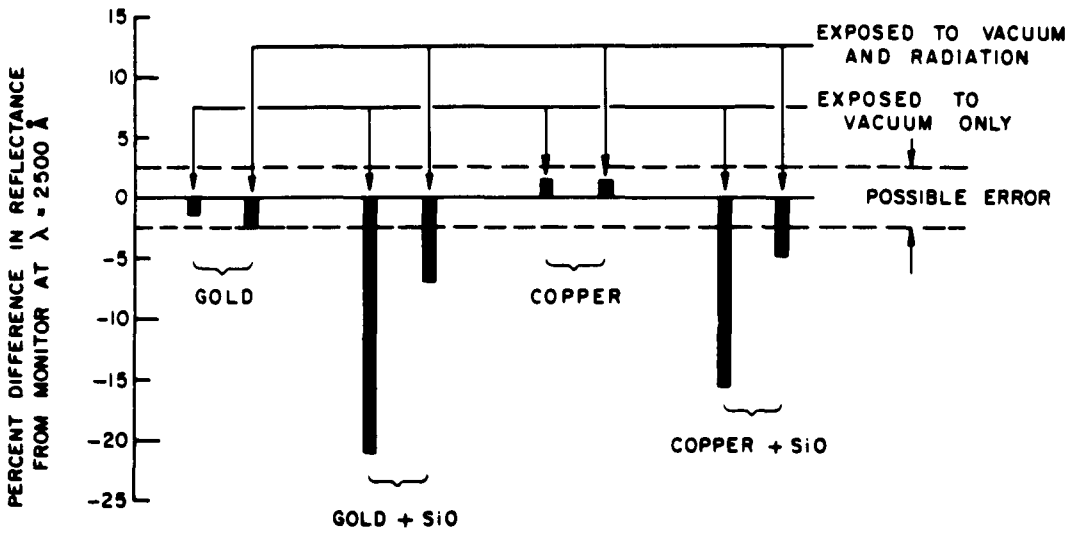

FIG. 26 THE EFFECT OF ULTRA-HIGH VACUUM AND/OR VACUUM ULTRAVIOLET RADIATION ON THE OPTICAL REFLECTANCE AT λ2500 OF VARIOUS MIRROR COATINGS

VIII. THE EFFECTS OF VACUUM ULTRAVIOLET RADIATION AND/OR ULTRAHIGH VACUUM ON THE ELECTRICAL RESISTANCE OF ALUMINUM OXIDE

This experiment was designed to evaluate any change in the electrical surface resistivity of an aluminum oxide disc as a result of its exposure to ultrahigh vacuum and vacuum ultraviolet radiation.

The sample was a circular disc of Coors AD86 ceramic (86 percent Al_2O_3 + MgO_2, SiO_2) which was mounted in the environmental chamber with one of its polished surfaces opposite the radiation source aperture. Two silver electrodes were vacuum coated onto this ceramic surface to allow attachment of leads for the measurement of the surface resistance. These parallel electrodes defined an interelectrode ceramic surface of 1 cm width. A metal shield was attached to each electrode to prevent their receiving any radiation. Otherwise, electrode effects which could obscure those arising from irradiation of the ceramic might have been introduced.

Electrical connection from the disc electrodes to the outside of the chamber was made via the electrical feedthrough header previously described in Section IV. The interelectrode surface resistance was measured with a Keithley Electrometer (Model 610A) which is capable of measuring resistances as high as 10^{14}ohms. The original resistance of the ceramic disc was of the order of 10^{10}ohms, while the insulation resistance of all leakage paths which were electrically in parallel with the disc was greater than 10^{14}ohms. This meant that any change in the ceramic resistance due to the effects of the chamber environment would not be shorted out and should be detectable.

1 Experimental Results

The first measurement of the ceramic resistance was with the disc in its original condition following fabrication. A value of order 10^{10}ohms was obtained utilizing the electrometer as an ohmmeter.

The actual value obtained was found to be dependent on the electrometer 'range' used which indicated that the surface resistance was a function of the measuring voltage across it. Thus, it was found that the resistance measured 2.8×10^{10} ohms with 28 volts acting and 5.0×10^{10} ohms with 5 volts acting. This was substantiated by using an external power supply and determining the resistance from current measurements with the electrometer. These yielded, e.g., a resistance value of 3×10^{9} ohms for an applied voltage of 300 volts. Finally, the resistance was determined by discharging a capacitor through it and measuring the time constant. Resistance values of 6.2×10^{9} ohms and 1×10^{10} ohms were found with initial capacitor voltages of 100 volts and 10 volts respectively. Evidently, all these measurements indicate a decrease of resistance with an increase in the applied voltage.

The measurements of the original ceramic resistance discussed above were performed before the disc was mounted in the chamber. A further measurement which was made external to the chamber was after the ceramic surface was cleaned by washing in distilled acetone. The resistance value then obtained is given in Table 2, together with the values observed in the chamber at various pressures, and before and after irradiation.

All the resistance values listed in Table 2 were recorded with the Keithley Electrometer used as an ohmmeter. The electrometer output was fed to a Beckman potentiometric strip chart recorder to allow graphical presentation of the resistance. Due to the long time constant of the measuring circuit, it was necessary to wait for periods of about 30 minutes for the resistance reading to attain its true equilibrium value. This fact, coupled with the dependence of the ceramic resistance on the chamber pressure, required that special precautions be taken to obtain good measurements.

The influence of the chamber pressure on the ceramic resistance is clear from examination of Table 2. Presumably, as the pressure was reduced, the resultant de-contamination of the ceramic surface led to an increase in its resistance.

TABLE 2

EXPERIMENTAL HISTORY OF CHANGE IN CERAMIC RESISTANCE

Ceramic Condition	Pressure mm Hg.	Resistance in Ohms			
		a	b	c	d
		x10^{10}	x10^{10}	x10^{12}	x10^{12}
Outside chamber, original condition	(760)	2.8	5.0		
Outside chamber, Acetone washed	(760)			4.3	
Inside chamber, before evacuation	(760)			5.4	
Inside chamber, evacuated	2×10^{-3}			~8	
Inside chamber, evacuated	1×10^{-3}			~9	~10
Inside chamber, evacuated	1×10^{-4}			$\leq$4	$\leq$10
Inside chamber, evacuated	4×10^{-8}			>10	
Inside chamber, chamber opened	(760)			8.5	
Inside chamber, evacuated	1.3×10^{-8}			>10	9
Inside chamber, evacuated	4×10^{-9}				5.6
Inside chamber, evacuated	2.2×10^{-9}				22
Inside chamber, before irradiation*	1.9×10^{-9}				~18
Inside chamber, after irradiation*	1.8×10^{-9}				~21
Inside chamber, chamber opened	(760)			9.5	4.5

Electrometer Range Setting: a = 10^{9}, b = 10^{10}, c = 10^{11}, d = 10^{12}

* Irradiated with 100 pulses at 20 kv.

When the pressure was reduced to about 2×10^{-9} mm Hg the ceramic surface was subjected to 100 pulses of radiation, the source voltage being 20 kV. As each pulse was fired, the ceramic resistance instantaneously decreased its value, by at least 2 orders of magnitude in the case of a 20 kV pulse. This fact is illustrated in Fig. 27 which is reproduced from strip chart records of the electrometer output. One of the two records given in the figure is of the resistance decrease for 3 successive 14 kV pulses. The magnitude of the decrease is the same for each pulse which indicates that the source output is constant. The second record shown is of the resistance decreases for 3 pulses with increasing source voltages, viz., 10 kV, 15 kV, and 20 kV. It is seen that the magnitude of the resistance decrease is directly related to radiation pulse energy. To obtain the records shown in Fig. 27, the electrometer was externally adjusted after each pulse so that its reading immediately returned to the true value of the ceramic resistance. Otherwise, as noted previously, the long effective time constant of the circuit meant waiting for prohibitively long periods of time following each pulse.

As indicated in Table 2, there was no significant change in the measured value of the ceramic resistance after being subjected to 100 pulses of 20 kV radiation. Since it has been definitely established that the ceramic surface conductivity increased during the time the radiation was incident, it must be concluded that the current carriers created in the presence of the radiation were transient in nature and were neutralized by recombination mechanisms once the flux decreased. No permanent change in the surface resistivity of the aluminum oxide insulator was observed during the experiment.

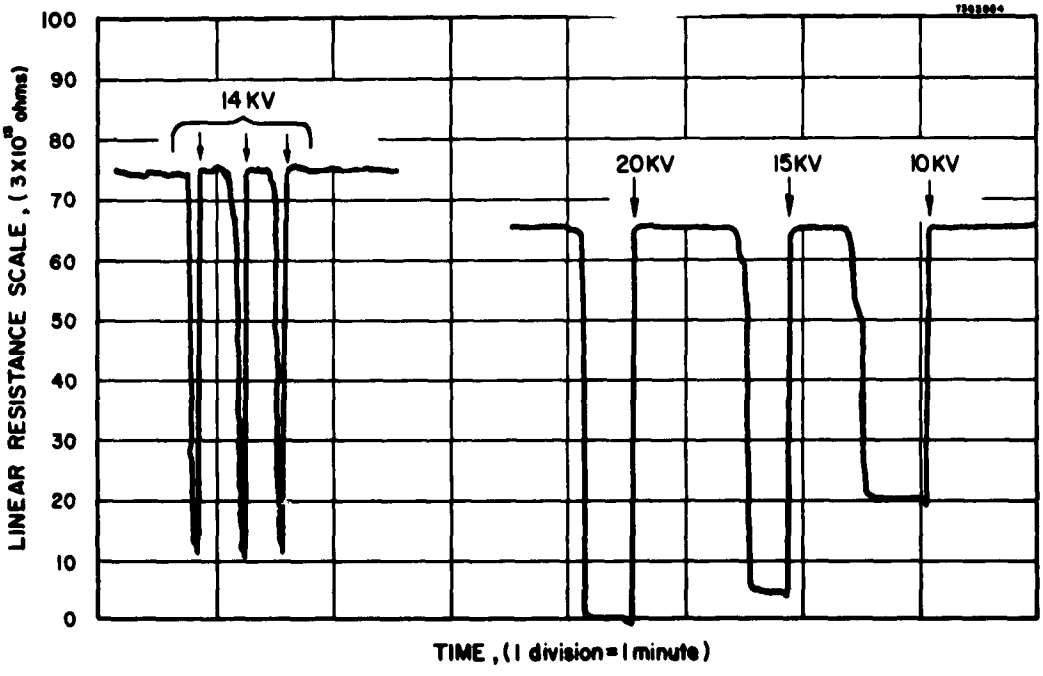

FIG. 27 STRIP CHART RECORD SHOWING THE INSTANTANEOUS DECREASE IN THE ELECTRICAL RESISTANCE OF THE CERAMIC SURFACE DURING ITS EXPOSURE TO RADIATION PULSES OF VARIOUS ENERGIES

IX. CONCLUSION AND RECOMMENDATIONS FOR FURTHER WORK

As a result of the program of research and development carried out at Electro-Optical Systems under USAF Contract No. AF 33(616)-6488 an important research facility has been assembled. Its unique capability enables materials in a vacuum of order 10^{-9} mm Hg. to be irradiated with vacuum ultraviolet radiation.

The facility has been brought into operation with only one technical problem not completely solved. For optimum operation of the facility further work should be done to reduce the ejection of material from the radiation source or to trap such material externally. When a solution to this problem is found the radiation source can be operated at its full design power.

The exploratory environmental effects studies carried out to date in the facility, while necessarily limited in their scope, have yielded definite results. These are summarized in Table 3. The most noteworthy effect observed is the fact that the reflectance (λ2500) of the silicon monoxide overcoated metallic mirrors deteriorated less due to exposure to radiation and vacuum than due to vacuum exposure alone.

On the basis of the preliminary results summarized in Table 3, the following recommendations are made for immediate further work with the environmental facility:

1. A definitive study of the nature of the effects of vacuum and/or vacuum ultraviolet radiation on the physical and chemical properties of thin film dielectrics such as silicon monoxide.
2. A definitive study of the nature of the effect of vacuum and/or vacuum ultraviolet radiation on the electrical properties of insulators such as aluminum oxide.

TABLE 3

SUMMARY OF ENVIRONMENTAL EFFECTS STUDIES

MATERIAL	FORM	CHARACTERISTIC STUDIED	EFFECTS OBSERVED DUE TO ENVIRONMENTAL EXPOSURE (*)	
			VACUUM	RADIATION
Doped Silicon (Semiconductor)	Solar cell	Power output via current-voltage characteristic curve	Slight increase (T)	Indeterminate
Aluminum Oxide (Insulator)	Ceramic disc	Electrical resistance	~ 100% increase (T)	>98% decrease (T)
Gold (Metallic conductor)	Specular mirror	Optical reflectance	None (λλ4000-6500) None (λ2500)	None (λλ4000-6500) None (λ2500)
Copper (Metallic conductor)	Specular mirror	Optical reflectance	3.5% decrease (λ4200), (P) None (λ2500)	None (λλ4000-6500) None (λ2500)
Silicon Monoxide (Dielectric)	Thin film overcoat on gold mirror	Optical reflectance	None (λλ4000-6500) 21% decrease (λ2500), (P)	None (λλ4000-6500) 7% decrease (λ2500), (P)
Silicon Monoxide (Dielectric)	Thin film overcoat on copper mirror	Optical reflectance	3% decrease (λ4200), (P) 15.5% decrease (λ2500), (P)	None (λλ4000-6500) 5% decrease (λ2500), (P)

*(P) = Permanent change; (T) = Temporary (in vacuum) or Transient (during irradiation) change

In addition, it is recommended that the following topics be considered as suitable for future work with the environmental facility:

1. The experimental evaluation of the effect of the physical condition of a material on its photoelectric properties in the vacuum ultraviolet.
2. The experimental investigation of the nature of surface energy states at clean surfaces of pure materials through characteristic photon energy loss measurements on very thin films of controlled thickness.
3. The experimental evaluation of the photon sputtering concept.
4. The experimental evaluation of the effects of vacuum and/or vacuum ultraviolet radiation on the surface recombination velocity of a semiconductor.
5. The effect of vacuum ultraviolet radiation on the formation of free radicals in prepolymer, simple organic, biological, and biochemical materials.

APPENDIX

SPECTROGRAPHIC INSTRUMENTATION

Two vacuum-type spectrographic instruments were purchased from the Jarrell-Ash Company for use during the development of the radiation source and detector.

One instrument is the Seya-Namioka Monochromator shown in Fig. 28. It is equipped with a 30,000 grooves per inch replica concave grating of 50 cm radius of curvature and which is blazed for λ1100. The instrument has an effective wavelength range of λλ500-3000 and is provided with a twelve speed wavelength scanning drive.

A camera is available for use with the monochromator. When substituted for the exit slit, it effectively converts the instrument into a spectrograph. Figure 29 shows a typical spectrogram obtained with the camera using Kodak SWR 35 mm film.

The second instrument is the Grazing Incidence Vacuum Spectrograph shown in Fig. 30 . The spectrograph is equipped with an original concave grating of 1 meter radius of curvature and with 30,000 grooves per inch. The ruling on this grating is designed to give relatively constant intensity over most of the wavelength range which is, theoretically, λλ0-3000.

A spectrogram of the emission of the pulsed radiation source obtained with the spectrograph on Kodak SWR 35 mm film is shown in Fig. 5.

FIG. 28 SEYA-NAMIOKA VACUUM MONOCHROMATOR

Wavelength Setting, λs

FIG. 29 SPECTROGRAM OF HELIUM DISCHARGE SOURCE RECORDED WITH SEYA-NAMIOKA VACUUM MONOCHROMATOR

FIG. 30 GRAZING INCIDENCE VACUUM SPECTROGRAPH BEING USED TO ANALYZE RADIATION FROM VACUUM ULTRAVIOLET RADIATION SOURCE. The operator is about to insert the film camera into the instrument

REFERENCES

1. W. C. Walker, N. Wainfan, and G. L. Weissler: Photoelectric Yields in the Vacuum Ultraviolet, J.A.P., 26, 1366, 1955

2. A. P. Lukirskii, M. A. Rumsh, and L. A. Smirnov: Measurement of the Photoelectric Yield for Ultrasoft X-Radiation, Optics and Spectroscopy, 9, 265, 1960

Aeronautical Systems Division, Dir/Materials And Processes, Physics Lab, Wright-Patterson AFB, Ohio Rpt Nr WADD-TR-60-371, Part II. A SOURCE AND DETECTOR OF RADIATION IN THE WAVELENGTH REGION 1500-50 ANGSTROMS SUITABLE FOR RADIATION EFFECTS STUDIES ON MATERIALS IN VACUO: A Study of Vacuum Ultraviolet Radiation Effects on Materials in Vacuo of Order 10^{-9} mm Hg. Final report, Dec 62. 79p. incl illus., tables, 2 refs.

Unclassified Report

This report describes a space environmental research facility whereby the effects of ultrahigh vacuum and/or vacuum ultraviolet radiation on materials can be experimentally evaluated. The facility consists of an environmental chamber of cylindrical dimensions 18" diameter x 18" depth, which is equipped with various functional and diagnostic controls, and with which is associated a vacuum

(over)

1. Space environmental research facility
2. Vacuum ultraviolet radiation source
3. Radiation detector

I. AFSC Project 7360 Task 736004
II. Contract AF 33(616) 6488
III. Electro-Optical Systems, Inc. Pasadena, Calif.
IV. H.R. Moore, H. Bernstein, R.S. Reynolds
V. Aval fr OTS
VI. In ASTIA collection

ultraviolet radiation source and a radiation detector. The radiation source is a pulsed plasma discharge which emits a line and continuum spectrum extending from the visible, through the vacuum ultraviolet, into the soft x-ray region. The radiation detector utilizes an open photoelectron multiplier tube which is mounted in the chamber for measurements of the radiation pulse energy. The environmental facility vacuum system includes a differentially pumped source-chamber connection and is capable of maintaining chamber pressures of order 10^{-9} mm Hg while the source is in operation. This report includes a description of the results of some exploratory studies of the effects of ultrahigh vacuum and/or vacuum ultraviolet radiation on the characteristics of a silicon solar cell, the electrical surface resistivity of aluminum oxide, and the optical reflectance of metallic mirror coatings.

Aeronautical Systems Division, Dir/Materials And Processes, Physics Lab, Wright-Patterson AFB, Ohio Rpt Nr WADD-TR-60-371, Part II. A SOURCE AND DETECTOR OF RADIATION IN THE WAVELENGTH REGION 1500-50 ANGSTROMS SUITABLE FOR RADIATION EFFECTS STUDIES ON MATERIALS IN VACUO: A Study of Vacuum Ultraviolet Radiation Effects on Materials in Vacuo of Order 10^{-9} mm Hg. Final report, Dec 62. 79p. incl illus., tables, 2 refs.

Unclassified Report

This report describes a space environmental research facility whereby the effects of ultrahigh vacuum and/or vacuum ultraviolet radiation on materials can be experimentally evaluated. The facility consists of an environmental chamber of cylindrical dimensions 18" diameter x 18" depth, which is equipped with various functional and diagnostic controls, and with which is associated a vacuum

(over)

1. Space environmental research facility
2. Vacuum ultraviolet radiation source
3. Radiation detector

I. AFSC Project 7360 Task 736004
II. Contract AF 33(616) 6488
III. Electro-Optical Systems, Inc. Pasadena, Calif.
IV. H.R. Moore, H. Bernstein, R.S. Reynolds
V. Aval fr OTS
VI. In ASTIA collection

ultraviolet radiation source and a radiation detector. The radiation source is a pulsed plasma discharge which emits a line and continuum spectrum extending from the visible, through the vacuum ultraviolet, into the soft x-ray region. The radiation detector utilizes an open photoelectron multiplier tube which is mounted in the chamber for measurements of the radiation pulse energy. The environmental facility vacuum system includes a differentially pumped source-chamber connection and is capable of maintaining chamber pressures of order 10^{-9} mm Hg while the source is in operation. This report includes a description of the results of some exploratory studies of the effects of ultrahigh vacuum and/or vacuum ultraviolet radiation on the characteristics of a silicon solar cell, the electrical surface resistivity of aluminum oxide, and the optical reflectance of metallic mirror coatings.

Aeronautical Systems Division, Dir/Materials And Processes, Physics Lab, Wright-Patterson AFB, Ohio Rpt Nr WADD-TR-60-371, Part II. A SOURCE AND DETECTOR OF RADIATION IN THE WAVELENGTH REGION 1500-50 ANGSTROMS SUITABLE FOR RADIATION EFFECTS STUDIES ON MATERIALS IN VACUO: A Study of Vacuum Ultraviolet Radiation Effects on Materials in Vacuo of Order 10^{-9} mm Hg. Final report, Dec 62. 79p. incl illus., tables, 2 refs.

Unclassified Report

This report describes a space environmental research facility whereby the effects of ultrahigh vacuum and/or vacuum ultraviolet radiation on materials can be experimentally evaluated. The facility consists of an environmental chamber of cylindrical dimensions 18" diameter x 18" depth, which is equipped with various functional and diagnostic controls, and with which is associated a vacuum

(over)

ultraviolet radiation source and a radiation detector. The radiation source is a pulsed plasma discharge which emits a line and continuum spectrum extending from the visible, through the vacuum ultraviolet, into the soft x-ray region. The radiation detector utilizes an open photoelectron multiplier tube which is mounted in the chamber for measurements of the radiation pulse energy. The environmental facility vacuum system includes a differentially pumped source-chamber connection and is capable of maintaining chamber pressures of order 10^{-9} mm Hg while the source is in operation. This report includes a description of the results of some exploratory studies of the effects of ultrahigh vacuum and/or vacuum ultraviolet radiation on the characteristics of a silicon solar cell, the electrical surface resistivity of aluminum oxide, and the optical reflectance of metallic mirror coatings.

1. Space environmental research facility
2. Vacuum ultraviolet radiation source
3. Radiation detector

I. AFSC Project 7360 Task 736004
II. Contract AF 33(616) 6488
III. Electro-Optical Systems, Inc. Pasadena, Calif.
IV. H.R. Moore, H. Bernstein, R.S. Reynolds
V. Aval fr OTS
VI. In ASTIA collection

Aeronautical Systems Division, Dir/Materials And Processes, Physics Lab, Wright-Patterson AFB, Ohio Rpt Nr WADD-TR-60-371, Part II. A SOURCE AND DETECTOR OF RADIATION IN THE WAVELENGTH REGION 1500-50 ANGSTROMS SUITABLE FOR RADIATION EFFECTS STUDIES ON MATERIALS IN VACUO: A Study of Vacuum Ultraviolet Radiation Effects on Materials in Vacuo of Order 10^{-9} mm Hg. Final report, Dec 62. 79p. incl illus., tables, 2 refs.

Unclassified Report

This report describes a space environmental research facility whereby the effects of ultrahigh vacuum and/or vacuum ultraviolet radiation on materials can be experimentally evaluated. The facility consists of an environmental chamber of cylindrical dimensions 18" diameter x 18" depth, which is equipped with various functional and diagnostic controls, and with which is associated a vacuum

(over)

ultraviolet radiation source and a radiation detector. The radiation source is a pulsed plasma discharge which emits a line and continuum spectrum extending from the visible, through the vacuum ultraviolet, into the soft x-ray region. The radiation detector utilizes an open photoelectron multiplier tube which is mounted in the chamber for measurements of the radiation pulse energy. The environmental facility vacuum system includes a differentially pumped source-chamber connection and is capable of maintaining chamber pressures of order 10^{-9} mm Hg while the source is in operation. This report includes a description of the results of some exploratory studies of the effects of ultrahigh vacuum and/or vacuum ultraviolet radiation on the characteristics of a silicon solar cell, the electrical surface resistivity of aluminum oxide, and the optical reflectance of metallic mirror coatings.

1. Space environmental research facility
2. Vacuum ultraviolet radiation source
3. Radiation detector

I. AFSC Project 7360 Task 736004
II. Contract AF 33(616) 6488
III. Electro-Optical Systems, Inc. Pasadena, Calif.
IV. H.R. Moore, H. Bernstein, R.S. Reynolds
V. Aval fr OTS
VI. In ASTIA collection